Readily Prepared Metallo-Supramolecular Triple Helicates Designed to Exhibit Spin-Crossover Behaviour

Floriana Tuna,[a] Martin R. Lees,[b] Guy J. Clarkson,[a] and Michael J. Hannon*[a]

Abstract: New dinuclear supramolecular cylinders have been designed to exhibit spin-crossover behaviour, a form of molecular bistability. This has been achieved within the framework of our imine-based approach to supramolecular architecture by switching from pyridylimine systems to imidazolimines. Spin-crossover behaviour is achieved while retaining the simplicity and ease-of-synthesis of our molecular design. The imidazole groups used also introduce additional NH groups that engage in hydrogen-bonding to anions and solvents. In the case of the iron(II) tetrafluoroborate complex this hydrogen bonding links supramolecular cylinders into an extended two-dimensional array. Consistent with this, a sharper spin-crossover transition is observed for this compound than for the corresponding hexafluorophosphate salt. More subtle anion effects are indicated in the perchlorate salt which gives a two-step spin conversion, thereby displaying tristability.

Keywords: helical structures · N ligands · noncovalent interactions · spin crossover · supramolecular chemistry

Introduction

The use of metal–ligand interactions to assemble sophisticated supramolecular architectures is a powerful tool and a topic of considerable interest.[1] Achievements have included the deliberate design of catenanes and rotaxanes,[2] knots,[3] helices,[4] grids[5] and racks.[6] Such arrays have architectures and shapes not readily accessible by means of traditional covalent synthetic approaches and frequently are also objects with nanoscale dimensions. The applications of such arrays have primarily centred round the use of their size and shape. For example, the architecture may be designed such that it contains internal cavities, which can be used to recognise and/or encapsulate guest molecules, and this feature can be used for sensing, extraction or catalysis.[7] Alternatively the size and shape of the external surface may be used to recognise larger biomolecular binding sites (such as the major groove of DNA),[8] or the shape may be used to confer properties, such as liquid crystallinity, within macromolecules.[9]

Such metallo-supramolecular design not only leads to a defined overall architecture, but positions metal centres at precise locations within the array. Moreover these metal centres are frequently coupled (mechanically and/or electronically) by the bridging ligands. This is attractive for potentially controlling or encoding properties within a material. Indeed such ability to precisely position metal centres within a defined array is a key requirement in the field of molecular magnetism.[10] Of particular interest within that field is the spin-crossover phenomenon.[11] The fascination with spin-crossover compounds arises because they possess at least two stable states (for a mononuclear system: the high and low spin arrangements of the d electrons) with distinct properties (magnetism, colour). Excitingly the compounds can be switched reversibly between these states in response to changes in the environment (temperature, light, pressure, anions etc.). This property can be used for either molecular switching or molecular memory and for this reason such materials might find ultimate application in the electronics and data-storage fields.[12]

The use of supramolecular chemistry to design such spin-crossover materials has focused primarily on using π-stacking and hydrogen bonding to link mononuclear spin-crossover centres together.[13,14] This can cause mechanical and/or electronic coupling of the centres and thereby modify the properties of the material (e.g., inducing cooperativity leading to an abrupt spin transition or hysteresis in the spin transition or giving multiple stable states) as structural changes

[a] Dr. F. Tuna, Dr. G. J. Clarkson, Dr. M. J. Hannon
Centre for Supramolecular and Macromolecular Chemistry
Department of Chemistry, University of Warwick
Gibbet Hill Road, Coventry, CV4 7AL (UK)
Fax: (+44) 2476-524112
E-mail: m.j.hannon@warwick.ac.uk

[b] Dr. M. R. Lees
Department of Physics, University of Warwick
Gibbet Hill Road, Coventry, CV4 7AL (UK)

Supporting information for this article is available on the WWW under http://www.chemeurj.org/ or from the author.

 DOI: 10.1002/chem.200400518

are propagated from one molecule to another, to the whole crystal.[15] The use of metallo-supramolecular architecture is less well established but very attractive, because of the potential extent of the inter-metallic mechanical coupling. Williams has reported spin crossover within an iron(II) benzimidazole helicate[16] and Lehn and Gütlich have studied a spin-crossover tetranuclear grid system based on Lehn's pyrimidine-linked polypyridyl ligands.[17] In Williams' system the metal centres are mechanically coupled and negative cooperativity is observed. In the Lehn/Gutlich system both mechanical and electronic coupling is possible and gradual incomplete spin-transitions are reported. Both architectures are assembled in solution simply by mixing the metal and ligand, as a result of careful matching of the ligand donors with the metal-coordination requirements. However, as with most metallo-supramolecular designs, the synthesis of the ligands does require multistep covalent synthesis to encode the design algorithm for the metals to read.

Much of our work in the area of metallo-supramolecular architecture has focused on developing routes to construct such sophisticated supramolecular architectures without the need for extensive ligand synthesis. In particular, we have championed the use of pyridylimine ligands, which have allowed us to assemble complex metallo-supramolecular arrays in one-pot reactions (either with or without solvent) from commercial aldehydes, amines and metal salts.[18–20] By removing the constraints of extended ligand synthesis, we have then been able to readily and systematically modify the systems to explore both the design features[19] and the properties[8] of such arrays. We were intrigued to see whether our approach could be applied to the task of designing metallo-supramolecular arrays containing spin-crossover centres. While pyridylimine iron(II) complexes are low spin at room temperature, the elegant work of Matsumoto and Tuchagues[14] led us to explore whether switching from pyridylimines to imidazolimines might allow us access to spin-crossover behaviour, while retaining the simplicity and ease-of-synthesis of our molecular design. We report now our initial studies in this area in which we have prepared dinuclear triple-helical arrays of bis-imidazolimine ligands and explored their spin-crossover behaviour.

We were further attracted to these imidazolimines because they provide additional hydrogen-bond donor units (NH) that will be located on the exterior of the architecture. These hydrogen-bonding sites are potential aggregation sites through which the architecture might be organised into a larger array and indeed through which information about changes in spin-state within one supramolecular unit might be relayed to another. Despite their widespread use to aggregate mononuclear metal complexes into larger arrays, examples of hydrogen bonds aggregating metallo-supramolecular architectures remain rare. Lehn has functionalised tetranuclear grid systems with a donor–acceptor hydrogen-bond system and obtained linear chains of grids,[21] Puddephatt has incorporated amide hydrogen-bond units into triangles[22] and we have used hydroxy groups to aggregate pyridylimine double-helices.[20] A hydroxy unit can behave either as a hydrogen-bond acceptor or donor and we showed that the selection of anion mediates whether the aggregation is simple hydrogen-bond aggregation (with half the OH groups acting as donors and half as acceptors) or anion-mediated hydrogen-bond aggregation (with the OH groups acting only as donors and the anions acting as acceptors). By contrast (unless deprotonated) the imidazole NH group can act only as an hydrogen-bond donor and anion-mediated hydrogen-bond aggregation might therefore be anticipated.

Results and Discussion

The ligand **L** was selected because the corresponding pyridylimine ligand gives dinuclear triple-helical complexes with octahedral metal ions[18] and these helical molecular cylinders bind to and coil DNA.[8] This architectural framework

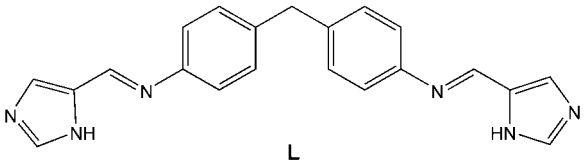

L

seemed an appropriate and interesting starting point from which to initiate our investigation into whether imidiazolimines could be used to introduce spin-crossover properties. Ligand **L** was prepared in 95% yield by mixing two equivalents of 4(5)-imidazolecarboxaldehyde and one equivalent of 4,4′-methylenedianiline in methanol. The ligand precipitated from the reaction mixture and was isolated by filtration. The microanalytical data, ^{1}H NMR spectrum and mass spectrum were consistent with the expected ligand formulation ($C_{21}H_{18}N_6$).

Coordination to iron(II) was achieved by stirring three equivalents of **L** with two equivalents of iron(II) chloride tetrahydrate in methanol for 40–45 minutes. Treatment with NH_4PF_6, NH_4BF_4 or $LiClO_4$ afforded orange polycrystalline salts $[Fe_2(\mathbf{L})_3]X_4$ (**1**: $X^{-}=PF_6^{-}$; **2**: $X^{-}=BF_4^{-}$; **3**: $X^{-}=ClO_4^{-}$). The same species were also obtained from solutions of 1:1 metal/ligand stoichiometry. The infrared spectra of **1**–**3** show absorptions characteristic of the coordinated ligands and the counterions (PF_6^{-}, BF_4^{-} or ClO_4^{-}) and partial microanalytical data are consistent with the dinuclear triple-stranded formulations. The mass spectra (FAB and electrospray) are similarly consistent with the dinuclear triple-stranded formulation. Peaks corresponding to the complex with associated anion are observed, such as $[Fe_2(\mathbf{L})_3X_3]^{+}$, and also peaks in which some of the NH units of the ligands have been deprotonated (possibly during the mass spectrometry process) such as $[Fe_2(\mathbf{L})_2(\mathbf{L}-H)X_2]^{+}$ and $[Fe_2(\mathbf{L})(\mathbf{L}-H)_2X]^{+}$.

Coordination of **L** to cobalt(II), nickel(II) and manganese(II) was achieved in a similar fashion by treating solutions of the ligand with the corresponding metal chlorides. The resulting complexes were isolated as the hexafluorophosphate salts $[M_2(\mathbf{L})_3][PF_6]_4$ (**4**: M=Ni; **5**: M=Co; **6**: M=Mn). Analytical and mass spectrometric data were analogous to those of the iron(II) complexes.

X-ray crystallographic studies: Crystals of all six complexes were obtained and the structures investigated by X-ray crystallography. Crystals of complexes **1**, **3**, and **4** were obtained from methanol. Crystals of **2** were obtained by diffusion of diisopropyl ether into a solution of **2** in acetonitrile, and diffusion of diethyl ether into an acetonitrile/acetone mix was used to obtain crystals of **5** and **6**. Data were collected at 180(2) K.

The cations in the six structures are very similar and all possess a dinuclear triple-helical architecture (Figure 1). In each structure the metal centres are in six-coordinate pseudo-octahedral coordination environments bound to three imidazolimine units from three different ligand strands. Each ligand strand binds to two metals and the ligands wrap around the metal–metal axis giving rise to the helical structure, both enantiomers of which are present in each structure. The imidazolimine units are approximately planar (torsion angles in the range 0–9°) and the phenylene units twisted with respect to that plane, affording CH···π interactions in the centre of the helix. The intermetallic separations are in the range 11.4–11.7 Å.

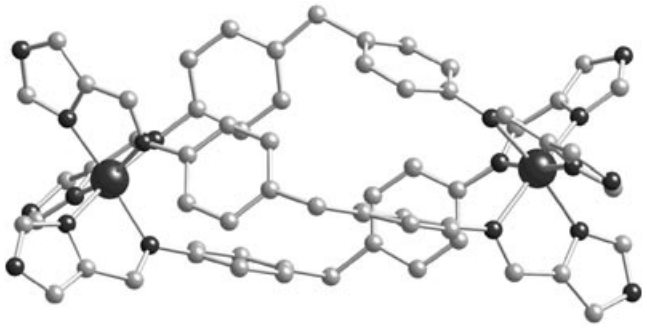

Figure 1. The structure of the triple-helical cation in complex **3**, $[Fe_2(\mathbf{L})_3][ClO_4]_4$. Hydrogens are omitted for clarity. The structures of the cations in complexes **1**,**2** and **4**–**6** are analogous.

Table 1. Selected bond lengths [Å] and bond angles [°] for complexes **1**–**6**.

	Metal	$M-N_{imidazole}$	$M-N_{imine}$	Bite angle
1	Fe1, Fe1a	1.980(6)	2.013(6)	81.1(3)
		1.952(7)	2.018(6)	80.1(3)
		1.976(6)	2.052(6)	80.0(3)
2	Fe1	2.011(7)	2.043(7)	80.0(3)
		2.000(7)	2.053(7)	79.7(3)
		1.994(7)	2.066(7)	80.3(3)
	Fe2	2.126(8)	2.250(7)	76.3(3)
		2.162(7)	2.222(7)	75.8(3)
		2.138(8)	2.194(8)	77.8(3)
3	Fe1	2.013(10)	2.114(10)	78.9(4)
		2.034(11)	2.103(11)	77.7(5)
		2.013(10)	2.137(11)	78.4(4)
	Fe2	2.118(13)	2.203(12)	75.6(5)
		2.075(12)	2.177(10)	75.9(4)
		2.094(11)	2.177(10)	77.2(4)
4	Ni1, Ni1a	2.036(6)	2.141(5)	78.9(2)
		2.045(5)	2.182(5)	78.7(2)
		2.062(6)	2.122(5)	79.2(2)
5	Co1	2.088(7)	2.188(7)	77.2(3)
		2.093(7)	2.183(6)	77.6(3)
		2.101(7)	2.227(7)	78.1(3)
	Co2	2.089(7)	2.206(7)	78.0(3)
		2.106(7)	2.222(7)	77.3(3)
		2.106(7)	2.196(6)	77.4(3)
6	Mn1	2.227(6)	2.303(6)	74.2(2)
		2.186(6)	2.337(5)	74.6(2)
		2.206(6)	2.336(6)	74.6(2)
	Mn2	2.204(7)	2.332(6)	74.6(2)
		2.202(6)	2.306(6)	74.9(2)
		2.198(6)	2.277(6)	74.8(2)

Table 2. Comparison of the dimensions [Å] of the helical cations in complexes **1**–**6**.

	1	**2**	**3**	**4**	**5**	**6**
M···M distance	11.3962(21)	11.5556(22)	11.5837(27)	11.5368(16)	11.5401(17)	11.6605(17)
length[a]	16.24	16.14	16.22	16.26	16.33	16.40
helical pitch	29.1	29.7	29.8	29.8	30.9	32.0
radius[b]	4.29	4.34	4.31	4.32	4.40	4.44

[a] Length is measured as the distance along the helical axis between the centroids derived from the three nitrogen atoms of the imidazole NHs at each end of the cylinder. [b] Radius is measured as the average of the distance of the three central carbon atoms (from the CH_2 groups) to their centroid.

Bond lengths and angles are collected in Table 1. For the iron(II) hexafluorophosphate salt (**1**), the two metal centres are crystallographically equivalent and the bond lengths indicate that both metal centres are low spin. In the tetrafluoroborate salt (**2**), the two metal centres are non-equivalent and the bond lengths indicate that one metal centre is low spin, while the other is high spin. For the perchlorate salt (**3**), the two centres are non-equivalent, but the bond lengths are intermediate between the expected high and low spin limits, perhaps indicating that the spin transition is in progress for this salt. The metal–ligand bond lengths for the cobalt(II) (**5**) and manganese(II) (**6**) complexes are consistent with high-spin configurations.

The dimensions of the six cylindrical triple-stranded helical cations are very similar (Table 2). Their overall length is ~18 Å (H···H) and the radius (to H) is ~4.9 Å. These supramolecular cylinders are close to 2 nm in length and 1 nm in diameter and thus are similar to the pyridylimine cylinders that we have previously characterised. Although the manganese cylinder is slightly longer than the others the difference is small, in the range 1–2%. This small increase in length is associated with a small decrease in the extent to which the ligands wrap around the helical axis and these two small effects combine to lead to the more noticeable lengthening (~7%) in helical pitch. Since the M–N bond lengths in the manganese(II) complex are ~10% greater than those in the iron(II) and nickel(II) conplexes, it is apparent that the choice of octahedral metal, and differences in bond lengths (expected for high- and low-spin configurations) cause only small perturbations to the size and shape of the cylinder structure.

To probe the effect on the micro-architecture of the triple helicates of imidazolimine units, it is pertinent to compare the structures of these new imidazolimine triple helicates

with those of the pyridylimine triple helicates.[18] To exclude possible effects of spin transitions, the comparison herein focuses on the d^8 nickel(II) helicates, in which such effects are negated. An overlay of the structures of the complexes of nickel(II) with the imidazolimine and pyridylimine ligands is shown in Figure 2. The overlay reveals that the cations are

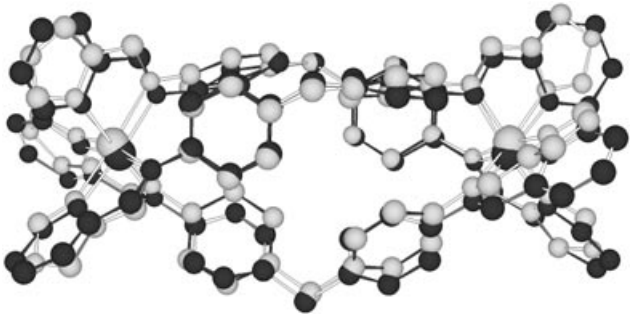

Figure 2. Overlay of the structures of the cations in the complexes of nickel(II) with the imidazolimine and pyridylimine[18] (shaded) ligands. Hydrogens are omitted for clarity.

structurally very similar. Clearly the replacement of the six-membered pyridine with the five-membered imidazole causes some small difference at the ends of the helicate, but this does not dramatically affect the length or the diameter of the helix. The aryl rings in the centre of the helicate form CH···π contacts as in the parent pyridylimine systems and this is illustrated in Figure 3. These interactions may contrib-

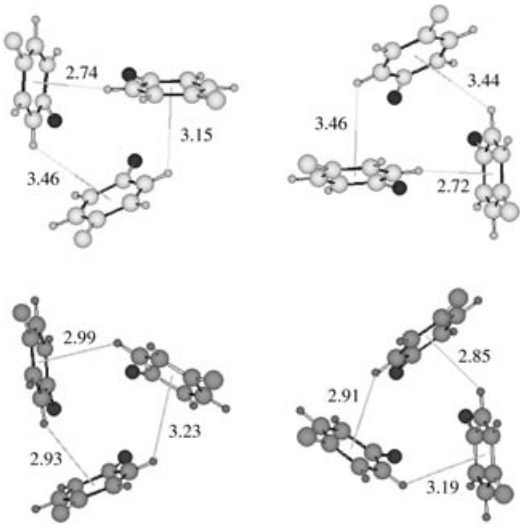

Figure 3. Comparison of the orientation of the phenylene rings in the cationic complexes of nickel(II) with the imidazolimine and pyridylimine[18] (shaded) ligands. Distances quoted are in Å.

ute to the stability of the structure. The precise orientation of the rings is slightly different in the imidazolimine system allowing one shorter contact at the expense of a lengthening of one of the other contacts.

Hydrogen-bonding interactions of the imidazole units in the solid-state: An attraction of the imidazole binding motif is that the imidazole NH units have potential to engage in hydrogen-bond interactions outside the cylinder structure, through which the cylinders might be organised into larger arrays and indeed through which information about changes in spin-state within one supramolecular unit might be relayed to another. This is indeed the case and an analysis of the contacts for each complex is presented below.[23]

Complex **1**: The two ends of the helix are identical. All three NH groups at each end engage in hydrogen bonding (Figure 4). The first group forms a hydrogen bond to a

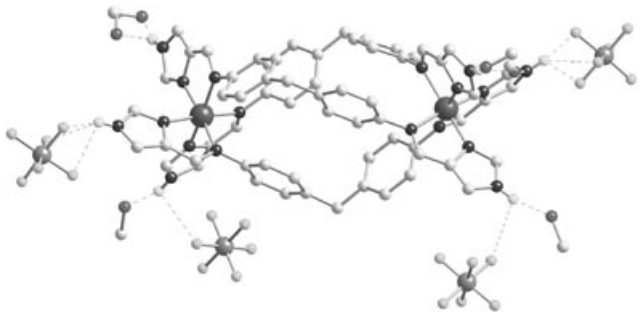

Figure 4. Hydrogen-bonding interactions to the NH groups in the triple-helical cation in complex **1**. For clarity only the NH protons are shown.

methanol solvent molecule (O···HN 1.93 Å) with a long interaction with a hexafluorophosphate anion (F···HN 2.85 Å). The second forms three hydrogen bonds to three fluorine atoms of one hexafluorophosphate anion (F···HN 2.35, 2.48, 2.78 Å). The third interacts with an additional methanol solvent molecule that is disordered over two sites (O···HN 1.96, 2.02 Å).

Complex **2**: All six NH groups engage in hydrogen bonding (Figure 5). The hydrogen-bond pattern at each end of the helix is very similar. At each end, one NH group forms a hydrogen bond to a water molecule (O···HN 1.92, 1.99 Å). The remaining two NH groups at each end form pairs of hydrogen bonds to two tetrafluoroborate anions (F···HN 2.16, 2.37; 2.32, 2.51; 2.17, 2.33; 2.30, 2.47 Å).[24] These pairs of tetrafluoroborate anions bridge between two helicates and in this way a two-dimensional network is assembled.

Complex **3**: All six NH groups engage in hydrogen bonding and the hydrogen-bond pattern at each end of the helix is slightly different (Figure 6). At one end, the first NH group forms a hydrogen bond to a methanol solvent molecule (O···HN 1.96 Å) with an additional long interaction to a perchlorate oxygen atom (O···HN 2.89 Å). The second NH group interacts with two oxygen atoms of a perchlorate anion (O···HN 2.04, 2.71 Å). The third forms a hydrogen bond to a water solvent molecule, which is disordered over three positions (O···HN 1.98, 2.09, 2.67 Å). At the other end of the helix, the first NH group forms a hydrogen bond to a methanol solvent molecule (O···HN 1.91 Å). This NH group also has a long contact to an oxygen atom in one orientation of a disordered perchlorate (O···HN 2.95 Å). The second NH group interacts with two oxygen atoms of a perchlorate anion (O···HN 1.99, 2.76 Å). The third interacts either with

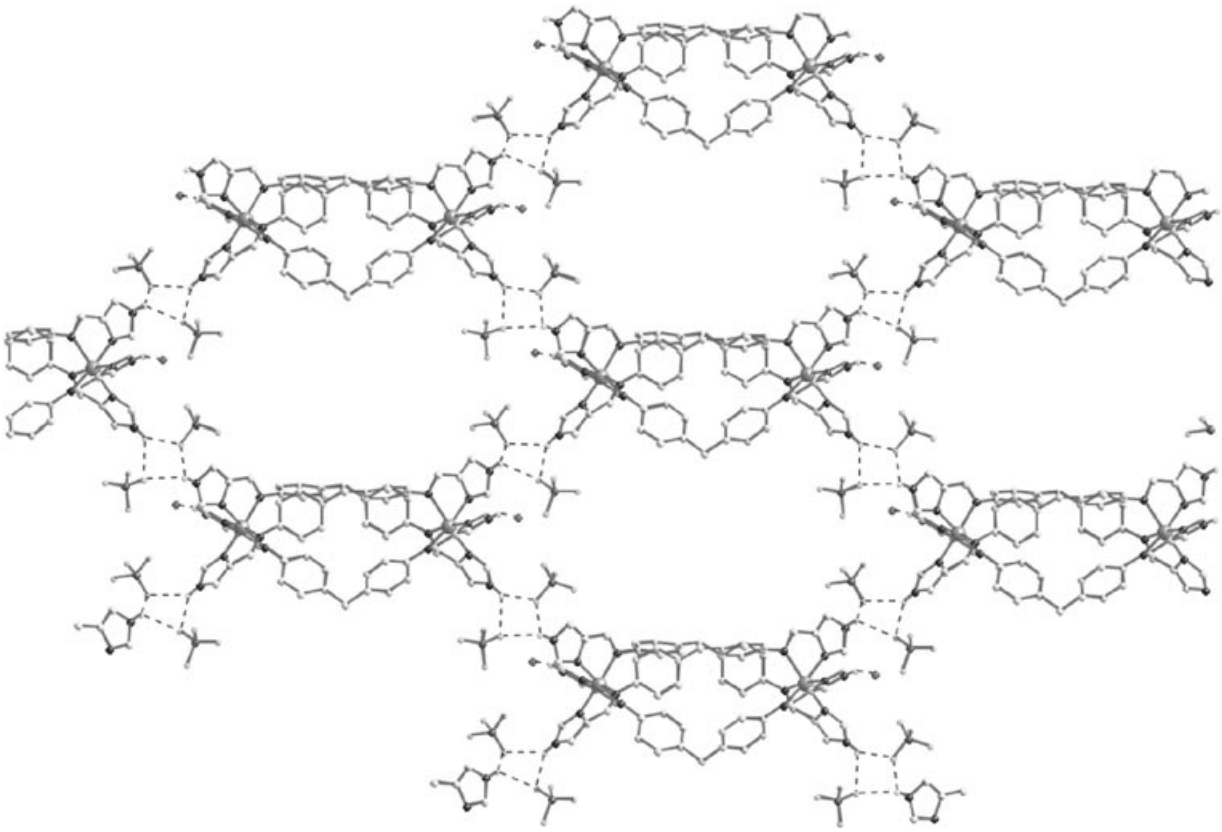

Figure 5. Hydrogen-bonding interactions to the NH groups in the triple-helical cation in complex **2**. For clarity only the NH protons are shown.

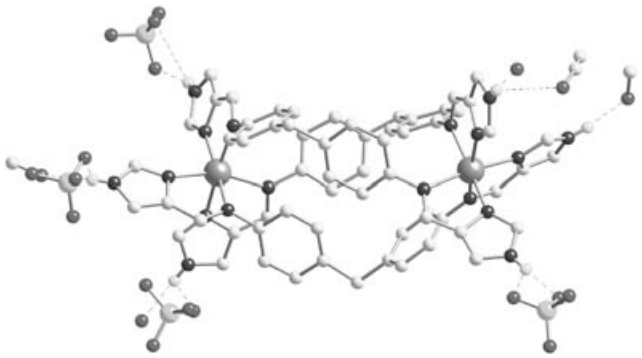

Figure 6. Hydrogen-bonding interactions to the NH groups in the triple-helical cation in complex **3**. For clarity only the NH protons are shown.

the disordered perchlorate (O···HN 2.29 Å), which formed a long contact to the first NH of another cylinder, or (when this perchlorate is in the alternate orientation) with a water solvent molecule (O···HN 2.10 Å), which is only occupied when the perchlorate is in this alternate orientation. This NH makes a further contact to a partially occupied methanol molecule (O···HN 2.57 Å).

Complex **4**: The crystals of complexes **1** and **4** are isomorphous apart from small differences in solvent content. Consequently it may be possible to grow mixed crystals. The hydrogen-bonding pattern in **4** is extremely similar to that observed in the corresponding iron(II) complex **1** with two disordered methanol solvent molecules replaced by two disordered water molecules. Further detail of the hydrogen bonding and a figure illustrating this are presented in the Supporting Information.

Complex **5**: All six NH groups engage in hydrogen bonding and the hydrogen-bond pattern at each end of the helix is different (Figure 7). At one end, the first NH forms a hydrogen bond to an acetone solvent molecule (O···HN 1.93 Å) with a long contact to a hexafluorophosphate anion (F···HN 2.96 Å). The second interacts with an additional acetonitrile molecule, which is only partially occupied (N···HN 2.16 Å), with a longer contact to a hexafluorophosphate anion (F···HN 2.74 Å). The third interacts with two fluorine atoms of a hexafluorophosphate anion (F···HN 2.12, 2.44 Å). Al-

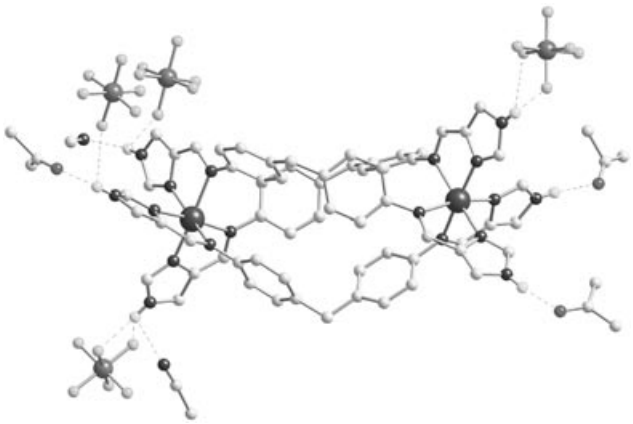

Figure 7. Hydrogen-bonding interactions to the NH groups in the triple-helical cation in complex **5**. For clarity only the NH protons are shown.

though this NH appears to have a long contact to an acetonitrile molecule (N···HN 2.89 Å), the interaction angle is close to 90° and we discount this as a hydrogen-bonding interaction. At the other end of the helix, two NH units form hydrogen bonds to one acetone solvent molecule each (O···HN 1.98, 2.01 Å). The third NH group interacts also with a hexafluorophosphate anion. This anion is disordered across two positions with two fluorine atoms interacting in the first orientation (F···HN 2.03, 2.52 Å) and three in the second (F···HN 2.31, 2.33, 2.52 Å).

Complex **6**: The crystals of **5** and **6** are pseudo-isomorphous, with almost identical crystal packing, apart from the variation in anion and solvent positions. (Although the crystal of complex **3** also has a very similar unit cell, the orientation of the cation within the cell is different). In complex **6**, all six NH groups engage in hydrogen bonding and the hydrogen-bond pattern at each end of the helix is different (Figure 8).

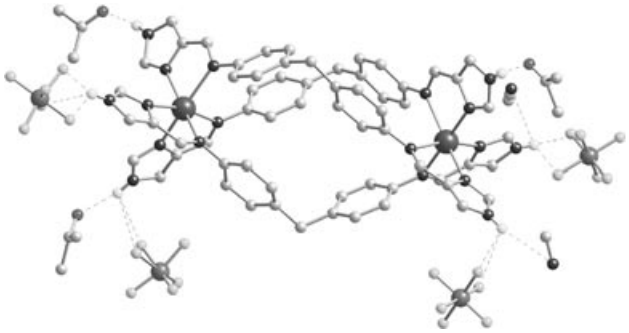

Figure 8. Hydrogen-bonding interactions to the NH groups in the triple-helical cation in complex **6**. For clarity only the NH protons are shown.

At one end, two NH groups form hydrogen bonds to acetone solvent molecules (O···HN 2.03; 2.01 Å), with one of these NH groups forming additional long contacts to a hexafluorophosphate anion. This anion is disordered over two sites and depending on its orientation makes either one (F···HN 2.78 Å) or two (F···HN 2.81, 2.93 Å) long contacts. (In the former case there is an additional long contact from this anion to the other end of an adjacent cylinder.) The third NH group interacts with a further hexafluorophosphate anion, which again is disordered over two orientations making either two (F···HN 2.02, 2.45 Å) or three (F···HN 2.30, 2.32, 2.45 Å) contacts to the NH group. At the other end of the helix, two NH groups interact each with two fluorine atoms of a hexafluorophosphate anion (F···HN 2.12, 2.31; 2.75, 2.91 Å). In both cases there are additional short contacts to acetonitrile solvent molecules (N···HN 2.94; 2.73 Å), although as in the cobalt(II) structure the angles are close to 90° and we discount these as hydrogen-bonding interactions. The third NH group forms a hydrogen bond to an acetone solvent molecule (O···HN 1.95 Å). There is a further long contact (F···HN 2.92 Å) to one orientation of a disordered anion. This anion is that mentioned above as bound to the other end of an adjacent cylinder and forming one or two interactions with that end of the cylinder. In this orientation, that anion bridges and links the cations into one-dimensional chains.

Although the precise hydrogen-bonding motifs differ in each complex, common themes are apparant: In all six structures, all four anions form hydrogen-bond contacts to the imidazole NH groups. In each structure, the hydrogen bonding to the anions is supplemented by hydrogen bonding to oxygen donor solvents, (methanol, water, and acetone). Where there are contacts to both an oxygen donor and an anion (i.e., F from PF_6 and BF_4), the imidazole NH group shows a preference for the oygen atom with that contact usually the shorter. All six NH units are engaged in hydrogen-bonding in all of the structures. Only in the BF_4 salt do anions bridge between NH groups. This is most probably because of the relatively high ratio of anions to complex (4:1) in these compounds. However, in the BF_4 structure this bridging effect does enable the hydrogen bonding through the imidazole groups to position the cylinders with respect to each other and links the cylinders into a remarkable network structure.

Aside from these hydrogen-bond interactions, the principal additional noncovalent interactions in the crystal are CH···π interactions. For structures **1** and **3–6** these lead to a common packing motif of the cylinders in the crystal and this is illustrated in Figure 9 for the iron(II) hexafluorophosphate complex **1**. In this complex CH···π interactions from the imine CH protons to the imidazole rings of adjacent cylinders (CH···centroid 3.38, 3.52 Å) and from the imidazole CH protons (those at the 2-position, located between the imidazole nitrogens) to the phenyl rings of adjacent cylinders (CH···centroid 2.98, 3.47 Å) link the cylinders into a three-dimensional network. Similar packing and distances are observed for complexes **3–6**. The involvement of these particular two sets of protons in CH···π interactions is consistent with their proximity to the heteroatoms.

For complex **2**, the same interactions link the hydrogen-bonded sheet structures together in layers through imidazole (2-position) CH to phenyl interactions (CH···centroid 2.86 Å) and imine CH to imidazole interactions (CH···centroid 3.28, 3.54 Å) with additional contacts from central CH_2 protons to an imidazole (CH···centroid 3.51 Å) also observed. This is illustrated in the Supporting Information. Thus in all six complexes, NH···X and/or CH···π interactions link the cylinders within the three-dimensional structure and these interactions could provide a potential pathway to relay information about changes in an individual cylinder to the bulk material.

Paramagnetic ^{1}H NMR spectroscopy: Compounds **1–5** were investigated by ^{1}H NMR spectroscopy in deuterated acetonitrile (see Table 3). Due to its low solubility, complex **6** was omitted from this study. As expected, the proton resonances were strongly affected by the unpaired electron density on the paramagnetic metal centres (Figure 10). The ensuing electronic magnetic moment causes the broadening of the ^{1}H NMR signals and prevents resolution of any hyperfine coupling. The proton resonances are extended over a large chemical shift range (−20 to 235 ppm), as anticipated for paramagnetic samples. The data and tentative assignments are presented in Table 2. Assignments are based up on the intensities, proximity of the protons to the paramagnetic

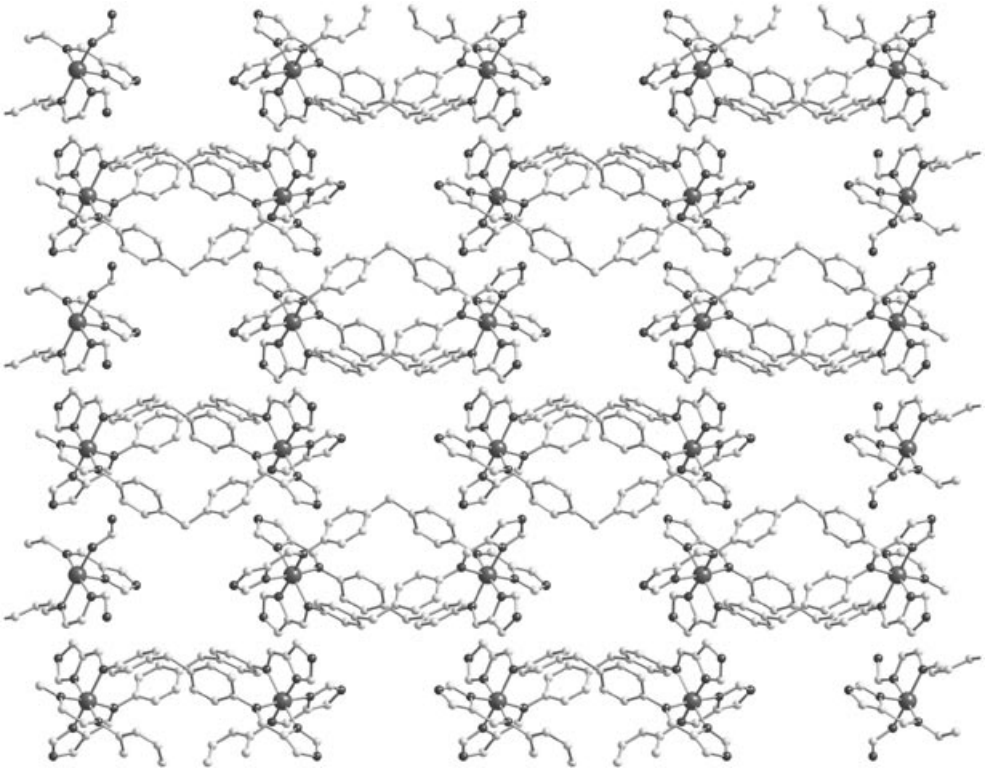

Figure 9. Solid-state packing of the cylindrical cations in the crystal structure of complex **1**. Hydrogen atoms, anions and solvents are omitted for clarity. The packing in complexes **3**–**6** is analogous.

Table 3. Room temperature, 500 MHz ^{1}H NMR data[a] for complexes **1**–**5**.

Assignment[b]	Integ.[c]	**1**	**2**	**3**	**4**	**5**
H^2	1	158.3	159.2	158.3	229.0	235.0
N*H*	1	92.1	92.7	92.1	93.1	99.6
H^{im}	1	42.5	42.9	42.5	58.7	23.8
H^4	1	37.9	38.1	37.9	40.9	52.9
CH_2	1	24.7	24.8	24.7	27.5	22.1
H^{Ph}	2	14.6	14.7	14.6	15.4	2.0
$H^{Ph'}$	2	−5.6	−5.7	−5.6	−6.7	−19.1

[a] In CD_3CN, ppm. [b] Tentative assignments. [c] Relative intensities.

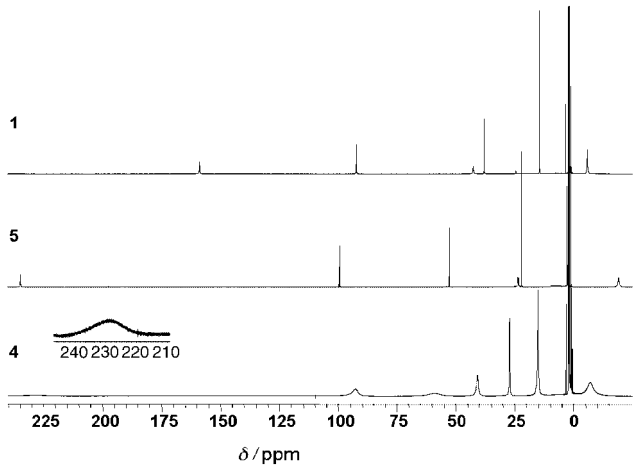

Figure 10. ^{1}H NMR spectra in CD_3CN solution at 298 K of complexes **1**, **4** and **5**. The inset is an expansion of the 230 ppm peak in complex **4**.

centre and observed line broadening (which is proportional to r^{-6}, whereby r is the distance between the nuclear and the electronic magnetic dipoles) and by comparison to high-spin iron(II)[25] and cobalt(II)[26] terpyridyl complexes and also with nickel(II) and cobalt(II) bipyridyl helicate complexes.[27] To identify the NH proton resonance, titration experiments with Et_3N were undertaken. In all cases, the disappearance of the ^{1}H NMR signal at approximately 90–100 ppm was observed upon addition of Et_3N.

The iron(II) complexes have also been studied at lower temperatures. As the temperature is decreased there is a decrease in intensity of the signals and at 233 K the signals become very weak (e.g., signal at ~165 ppm can no longer be resolved) and new peaks in the diamagnetic region can just be discerned in the baseline. This is consistent with a spin transition in solution, which is not completed within the available temperature range.

Electronic and magnetic properties: The electronic spectra of compounds **1**–**6** were recorded at room temperature in both acetonitrile and in the solid state. The solution spectra were recorded in the range 200–1100 nm in two different concentration ranges, so that the extinction coefficients of both the intense ligand bands and weaker metal-ion d–d transitions could be determined. The solid-state electronic spectra were recorded by the diffuse reflectance technique in the range 380–1200 nm.

The spectral features of the iron(II) compounds **1**–**3** are very similar to each other, and clearly indicate the presence of octahedral high-spin iron(II) chromophores. The diffuse

reflectance spectra each show a band centred at ~11200 cm^{-1} (893 nm), which is assigned to the $^5E \leftarrow {}^5T_2$ spin-allowed d–d transition of the iron(II) ion, along with a more intense peak at ~21250 cm^{-1} (470 nm), which may be due to a metal-to-ligand charge-transfer (MLCT) transition. Similarly, the UV-visible spectra in acetonitrile exhibit a weak broad band in the region 810–835 nm ($\varepsilon = 10$–$12\,M^{-1}cm^{-1}$), assigned to the $^5E \leftarrow {}^5T_2$ transition, along with a more intense band at 440 nm ($\varepsilon = 1400\,M^{-1}cm^{-1}$), assigned (by comparison with mononuclear iron(II) imidazolimine compounds[14]) as MLCT. Two very intense peaks are observed at approximately 32200 (310 nm; $\varepsilon \sim 53500\,M^{-1}cm^{-1}$) and 35700 cm^{-1} (280 nm; $\varepsilon \sim 58200\,M^{-1}cm^{-1}$), respectively, and they are assigned to π–π* transitions of the ligand. According to the literature data,[25,28] the $^1T_1 \leftarrow {}^1A_1$ and $^1T_2 \leftarrow {}^1A_1$ transitions associated to a low-spin $\{Fe^{II}N_6\}$ chromophore would be expected at about 380 and 550 nm, respectively, with a molar extinction coefficient of approximately $30\,M^{-1}cm^{-1}$. Such bands are not observed.

The electronic spectra of the cobalt(II) complex (**5**) also provide support for the existence of a high-spin six-coordinate chromophore (which is also consistent with both the X-ray data and the large downfield shift of some of the ^1H NMR resonances[26]). The solid-state spectrum displays two bands centred at 9170 (1090 nm) and 20280 cm^{-1} (493 nm), which are assigned to the $^4T_2 \leftarrow {}^4T_1$ and $^4T_1(P) \leftarrow {}^4T_1$ spin-allowed d–d transitions, respectively. The solution spectrum shows a weak ligand-field band at 490 nm ($\varepsilon = 42\,M^{-1}cm^{-1}$), along with two intense peaks at 285 ($\varepsilon = 55600\,M^{-1}cm^{-1}$) and 318 nm ($\varepsilon = 38250\,M^{-1}cm^{-1}$) corresponding to the π–π* transitions of the ligand.

Two ligand-field bands of moderate intensity are also present in the diffuse reflectance spectrum of nickel(II) complex, **4**. They are located at 10500 (952 nm) and 16650 cm^{-1} (600 nm) and are due to the spin-allowed transitions $^3T_2 \leftarrow {}^3A_2$ and $^3T_1(F) \leftarrow {}^3A_2$, respectively (assuming the *O* symmetry for the hexacoordinated nickel(II) chromophores). Interestingly, the second band is split into two components (16000 and 17060 cm^{-1}, respectively). The asymmetric feature of this band may be understood as arising from the non-equivalency of the nickel(II) chromophores or the splitting of the T state in lower symmetry. In the latter case, the spectral components correspond to the $^3B_1 \leftarrow {}^3A_2$ and $^3E \leftarrow {}^3A_2$ spin-allowed transitions, respectively. In solution, the band due to $^3T_2 \leftarrow {}^3A_2$ transition (554 nm; $\varepsilon = 24\,M^{-1}cm^{-1}$) is no longer split, but the electronic spectrum still supports a possible deformation of the octahedral coordination sphere of the nickel(II) ions. The first ligand-field band exhibits a maximum at 900 nm ($\varepsilon = 25\,M^{-1}cm^{-1}$) with a shoulder on its low-energy side. This result is in agreement with the crystal structure of **4**, which reveals that the six Ni–N bonds are non-equivalent. The ligand π–π* absorptions appear at 262 ($\varepsilon = 48300\,M^{-1}cm^{-1}$) and 308 nm ($\varepsilon = 66200\,M^{-1}cm^{-1}$).

The electronic spectra of compound **6** are less informative, because all the d–d transitions for high-spin manganese(II) chromophores are spin-forbidden. This compound is yellow (the ligand itself is white) and its UV-visible spectrum measured in acetonitrile shows two intense bands located at 267 ($\varepsilon = 51600\,M^{-1}cm^{-1}$) and 318 nm ($\varepsilon = 112000\,M^{-1}cm^{-1}$), the latter presenting a much higher extension coefficient than any of the other compounds studied herein. This could suggest a possible overlap of this ligand-based absorption band with one of charge-transfer origin. To investigate this possibility, we recorded the solid-state spectra of compounds **5** and **6** in the region 280–800 nm, and compared their spectral features; the manganese(II) spectrum displays a broad and intense band in the UV region, with a maximum at 357 nm and a shoulder at 335 nm, whereas the cobalt complex exhibits a intense peak at 335 nm, and a d–d band in the visible region.

Variable-temperature magnetic susceptibility measurements were carried out on polycrystalline samples of complexes **1–6** in the temperature range 1.8–340 K under an applied magnetic field of 1000 G. The $\chi_M T$ versus T plots (χ_M denoting the molar magnetic susceptibility) are given in Figure 11.

The room-temperature $\chi_M T$ value for $[Fe_2(L)_3][PF_6]_4$ (**1**) is 7.40 $cm^3 K mol^{-1}$, which corresponds to that of two magnetically uncoupled octahedral iron(II) centres with $^5T_2$ ground state and a calculated *g* term of 2.22. As the temperature is lowered down to 55 K, the $\chi_M T$ product decreases continuously (Figure 11), exhibiting a slight inflexion around 165 K. At this temperature, $\chi_M T$ is about 3.57 $cm^3 K mol^{-1}$, and corresponds to what is expected when 50% of the iron(II) ions undergo a thermally-induced spin conversion from the high-spin $^5T_2$ to the low-spin $^1A_1$ electronic state. The further de-

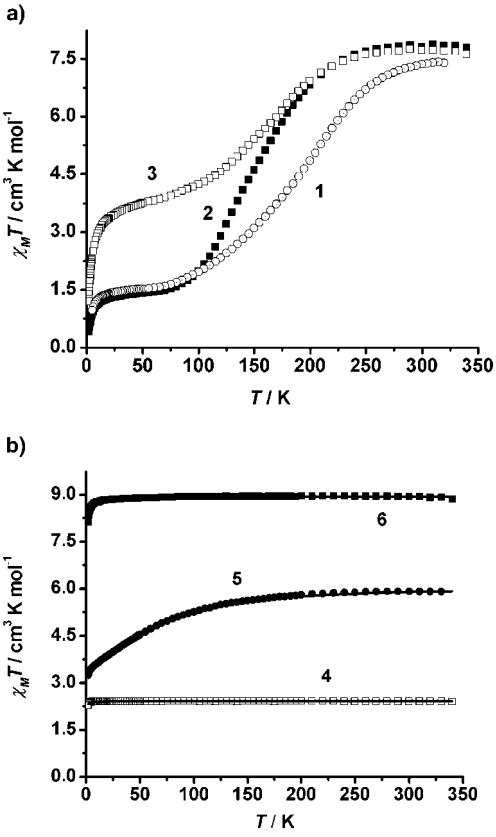

Figure 11. Magnetic susceptibility $\chi_M T$ versus T plots for complexes **1–6**. a) The iron(II) complexes **1–3**. b) The manganese, cobalt and nickel complexes **4–6**; the solid lines are fits discussed in the text.

crease of $\chi_M T$ is consistent with around 30% of iron(II) ions undergoing $S=2 \leftrightarrow S=0$ spin-conversion. Between 55 and 20 K, $\chi_M T$ remains almost constant at 1.5 $cm^3 K mol^{-1}$, and then drops abruptly reaching 0.96 $cm^3 K mol^{-1}$ at 5 K. This small decrease at very low temperatures may be ascribed to zero-field splitting in the orbital singlet $S=2$ ground state, arising from the strongly distorted coordination sphere of the remaining high-spin iron(II) ions in **1**.

The dinuclear, triple helix $[Fe_2(L)_3][BF_4]_4$ (**2**) behaves essentially in a similar way as **1**; however, in this case the spin-conversion is more rapid. At room temperature, $\chi_M T$ is equal to 7.83 $cm^3 K mol^{-1}$, which is in the range of values expected for two non-interacting iron(II) centres with $^5T_2$ ground state ($g=2.28$). The $\chi_M T$ product remains almost constant when cooling to 250 K (Figure 11) and then decreases rapidly to reach the value of 1.90 $cm^3 K mol^{-1}$ at 100 K. As for **1**, in the middle of the transformation ($\chi_M T \sim$ 3.6–3.7 $cm^3 K mol^{-1}$) the slope of the $\chi_M T$ *vs* T curve diminishes and a slight inflexion is observed. The plateau observed in the temperature region 70–25 K corresponds to 1.40 $cm^3 K mol^{-1}$, suggesting an incomplete HS($S=2$)↔LS($S=0$) transition (HS = high spin, LS = low spin) with about 20% of high-spin molar fraction trapped at low temperatures. The subsequent dropping of $\chi_M T$ at temperatures below 25 K corresponds most probably to the occurrence of zero-field splitting of the remainder of high-spin iron(II) ions.

For $[Fe_2(L)_3][ClO_4]_4$ (**3**), the $\chi_M T$ product is 7.70 $cm^3 K mol^{-1}$ in the temperature range 340–260 K, consistent with 100% of iron(II) centres in the high-spin state and a g value of 2.26. As the temperature is lowered, $\chi_M T$ diminishes rapidly to reach the value of 3.81 $cm^3 K mol^{-1}$ at 60 K (Figure 11). Between 60 and 40 K, the $\chi_M T$ product remains almost constant, and finally drops rapidly down to 1.2 $cm^3 K mol^{-1}$ at 1.8 K. These features reveal an incomplete HS↔LS spin conversion occurring in two steps. The first $\chi_M T$ drop is consistent with around 50% of iron(II) ions undergoing $S=2 \leftrightarrow S=0$ spin conversion. The second $\chi_M T$ drop may be understood as arising from the combined effect of electronic spin crossover and zero-field splitting of the remainder of high-spin iron(II) ions. For all three iron(II) complexes, the measurements were carried out in both cooling and warming modes, but no hysteresis has been observed.

The dinuclear, triple helix $[Co_2(L)_3][PF_6]_4$ (**5**) exhibits a room-temperature $\chi_M T$ of 5.90 $cm^3 K mol^{-1}$, which exceeds the spin-only value expected (3.75 $cm^3 K mol^{-1}$) for two magnetically non-interacting cobalt(II) centres in the $^4T_1$ ground state with $g=2$. This deviation is the result of the spin-orbit coupling displayed by high-spin cobalt(II) ions in octahedral environment. As the temperature is lowered $\chi_M T$ decreases, reaching 3.24 $cm^3 K mol^{-1}$ at 1.8 K (Figure 11b). This decrease may be due to the intrinsic behaviour of cobalt(II) centres rather than to antiferromagnetic exchange interactions among these paramagnetic centres. However, the experimental data were analysed with an equation which takes into account possible weak interactions between cobalt(II) ions, as described below.

In addition to the lowering of symmetry due to the deformation of the octahedral coordination sphere of the cobalt(II) ions, the coupling of the first-order orbital momentum with the spin momentum partially removes the degeneracy of the ground and the excited states. This results in a energy spectrum for a high-spin cobalt(II) ion in which the two low-lying levels correspond to the $M_S = \pm {}^1/_2$ and $\pm {}^3/_2$ states. Taking into account the Zeeman perturbation resulting from the applied external field, the Hamiltonian describing this situation is given by Equation (1)[10] in which Δ is the energy gap between the states split by the deformation of the coordination sphere, k is the orbital reduction factor accounting for the effect of the metal–ligand bond on the orbital momentum, and λ is a spin-orbit coupling parameter.

$$\mathscr{H} = \Delta(L_z^2 - {}^2/_3) - ({}^3/_2) k \lambda L \cdot S + \beta[-({}^3/_2) k L + g_e S] \cdot \mathscr{H} \qquad (1)$$

It has been shown that the axial splitting parameter Δ can be used in both the trigonal and the tetragonal field.[29] The other symbols have their usual meanings. A model taking into account all these parameters to fit the experimental magnetic data would be over-parameterised. Therefore, it is usual to consider that Δ is large enough to have only the two lowest Kramer doublets thermally populated in the investigated temperature range. In this situation the Hamiltonian can be given by Equation (2), in which D is the zero-field splitting parameter, defined as the energy separation between the lowest and the second lowest Kramers doublets from the $^4T_{1g}$ term, and is taken to be positive when the doublet referring to $M_S = \pm {}^1/_2$ is lowest.

$$\mathscr{H} = D[S_z^2 - S(S+1)/3] + \beta g \cdot S \cdot \mathscr{H} \qquad (2)$$

The orbital momentum no longer appears, but its influence is incorporated into both D and g parameters. The expression of the molar magnetic susceptibility deduced from this Hamiltonian is given in Equation (3).[30] It considers the paramagnetic behaviour for the two independent cobalt(II) ions found in the molecular formula. Possible weak interactions between the cobalt(II) sites are considered through a Curie-Weiss parameter θ.

$$\chi_M = \frac{2N\beta^2 g^2}{3k(T-\theta)} \frac{1+9e^{-2D/kT}}{4(1+e^{-2D/kT})} + \frac{4N\beta^2 g^2}{3k(T-\theta)} \frac{4+\frac{3kT}{D}(1-e^{-2D/kT})}{4(1+e^{-2D/kT})} \qquad (3)$$

The parameters obtained by the simulation of the experimental data by using the above expression are $g=2.535 \pm 0.001$, $D=86.32 \pm 0.8$ cm^{-1} and $\theta=-0.28 \pm 0.01$ K, consistent with data of the literature for cobalt(II) complexes.[31] The solid line in Figure 11b was calculated with these values. A negative sign for θ is consistent with antiferromagnetic interactions between metal centres. However, the value of θ close to zero indicates that the magnetic coupling between the cobalt centres is negligible in the triple helix, as expected from the large Co···Co distance of 11.54 Å. It also suggests that there are no significant intermolecular magnetic interactions between the paramagnetic centres.

For the helix $[Ni_2(L)_3][PF_6]_4$ (**4**), the molar magnetic susceptibility data can be fitted using the Curie–Weiss law ($\chi_M = C/(T-\theta)$) with $C=2.42$ $cm^3 K mol^{-1}$ and $\theta=-0.07$ K

(Figure 11b). The Curie constant (C) is in agreement with the expected value for two nickel(II) ions with $S=1$ and $g=2.2$.

The manganese helix $[Mn_2(L)_3][PF_6]_4$ (**6**), which has a room-temperature $\chi_M T$ value of $8.94\,cm^3\,K\,mol^{-1}$, also follows simple Curie–Weiss behaviour with $\theta=-0.18$ K and $C=8.94\,cm^3\,K\,mol^{-1}$ (Figure 11b), and exhibits a g value of 2.02.

Conclusion

These studies clearly demonstrate that, as envisaged, switching from pyridylimines to imidazolimines does allow access to spin-crossover systems, while retaining the simplicity and ease-of-synthesis of our supramolecular design. Although the focus herein is on triple-helical cylindrical arrays, the same approach should allow spin-crossover properties to the range of different architectures that we have investigated.[19] The imidazole NH groups engage in hydrogen bonding, showing a marked preference for oxygen donors, although all of the anions participate in interactions with the NH groups. Perhaps because of the high ratio of anions to cation (4:1), only in the iron(II) tetrafluoroborate structure do we observe significant bridging through hydrogen bonding. Nevertheless this leads to a striking two-dimensional sheet structure in which planes of cations are linked together. More extensive hydrogen-bonded networks might arise from partial deprotonation of the NH groups[14] and this will be the subject of future studies. CH···π interactions link the individual cations (**1**, **3**–**6**) or the sheets (**2**) into three-dimensional networks.

The solid-state spin-crossover behaviour of the iron(II) complexes is strongly influenced by the selection of anion. The tetrafluoroborate salt **2** demonstrates a much sharper (more rapid) transition than the hexafluorophosphate salt **1** and this would be consistent with a positive cooperativity between cylinders transmitted through the extensive hydrogen-bond network in the BF_4 salt. The behaviour of the perchlorate salt **3** is both more intriguing and quite different from the behaviour of these other two iron(II) salts, with an incomplete HS↔LS spin conversion observed that occurs in two steps. This is despite the fact that in both the hexafluorophosphate and perchlorate salts, the packing of the cylinders is almost identical and the environment and hydrogen bonding of the NH groups are similar (except that there are F-bonded anions in the hexafluorophosphate salt and O-bonded anions in the perchlorate salt). It is notable that the X-ray structure of the tetrafluoroborate salt indicates a mixed high-spin, low-spin structure. It therefore appears that the mixed spin-state system can also be stable for this anion, but that perhaps the plateau of stability is very small; the effect of the perchlorate therefore may be to extend this stability plateau (rather than to induce it). Williams reports[16] that, in his helicate systems, mechanical coupling leads to negative cooperativity within the helix, leading to a stable mixed spin-state; this model would be consistent with the perchlorate data. For the perchlorate salt, it is possible that the NH hydrogen bonds to oxygen-donor anions do cause a significant difference in electronic behaviour at the metal or that the crystal structure of this salt is not representative of the bulk. While anion effects on spin-crossover are known in the literature, precise mechanisms for those anion effects have rarely been elucidated.[11]

Experimental Section

General: All reagents and solvents were purchased from commercial sources (Aldrich) and used without further purification. NMR spectra were recorded on Brüker DPX 400 and DRX 500 instruments by using standard Brüker software. FAB mass spectra were recorded by the Warwick mass spectrometry service on a Micromass AutoSpec spectrometer using 3-nitrobenzyl alcohol as matrix. Infrared spectra (KBr pellets) were measured with a Perkin–Elmer Paragon 1000 FTIR spectrometer. UV-visible measurements in solution were made by using a PU 8720 scanning spectrometer or a Jasco V-550 spectrophotometer and in the solid state by using a VSU-2P (Carl Zeiss) spectrometer (diffuse reflectance technique), with MgO as a standard. Microanalyses were conducted on a Leeman Labs CE44 CHN analyser by the University of Warwick Analytical service. Magnetic measurements were carried out on a Quantum Design MPMS-5S SQUID magnetometer. The diamagnetic corrections for the compounds were estimated using Pascal's constants, and magnetic data were corrected for diamagnetic contributions of the sample holder.

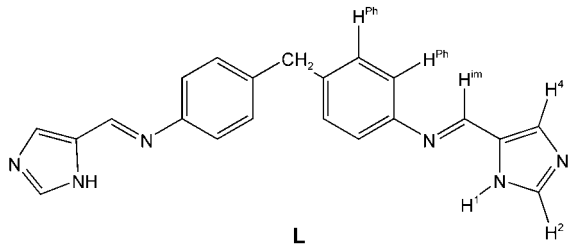

L

Preparation of L: 4,4′-Methylenedianiline (0.793 g, 4 mmol) and 4(5)-imidazolecarboxaldehyde (0.768 g, 8 mmol) were stirred in methanol (30 mL) for 10 min; two drops of glacial acetic acid were then added and the mixture was further refluxed for 2 h. An off-white solid precipitated and was collected by filtration, washed with methanol and dried in vacuo over P_4O_{10}. Yield: 95%; m.p. 260–261 °C; elemental analysis calcd (%) for $C_{21}H_{18}N_6$: C 71.2, H 5.1, N 23.7; found: C 70.9, H 5.1, N 23.5; MS (EI$^+$): m/z: 354 $[M]^+$; ^{1}H NMR (DMSO, 400 MHz, 300 K): $\delta=12.8$ (s, 1H; N*H*), 8.42 (s, 1H; H^{im}), 7.80 (s, 1H; $H^{2/4}$), 7.62 (s, 1H; $H^{2/4}$), 7.23 (d, $J=7.8$ Hz, 2H; H^{Ph}), 7.15 (d, $J=7.8$ Hz, 2H; H^{Ph}), 3.98 ppm (s, 1H; CH_2); IR data (KBr): $\tilde{\nu}=3060$ (sh), 3024 (m), 2970 (w), 2906 (w), 2832 (m), 2647 (w), 2589 (w), 1629 (vs), 1600 (s), 1546 (vw), 1502 (s), 1438 (m), 1414 (w), 1351 (w), 1331 (w), 1298 (w), 1222 (m), 1202 (w), 1170 (w), 1155 (sh), 1094 (m), 1014 (w), 991 (m), 918 (w), 874 (m), 845 (m), 808 (w), 787 (w), 752 (w), 710 (w), 622 (s), 601 (w), 539 (m), 480 cm^{-1} (vw).

Preparation of the complexes

$[Fe_2(L)_3][PF_6]_4$ (1): Ligand **L** (0.106 g, 0.3 mmol) and iron(II) chloride tetrahydrate (0.040 g, 0.2 mmol) were stirred in methanol (15 mL) for 45 min. The resulting orange solution was filtered through Celite and treated with methanolic ammonium hexafluorophosphate (excess). Slow evaporation of the solvent at room temperature yielded an orange microcrystalline product, which was collected by filtration, washed with cold methanol and dried in vacuo over P_4O_{10}. Yield: 67%; elemental analysis calcd (%) for $[Fe_2(C_{21}H_{18}N_6)_3][PF_6]_4\cdot 2H_2O$: C 42.2, H 3.2, N 14.1; found: C 41.9, H 3.0, N 14.0; MS (FAB): m/z: 1609 $[Fe_2(L)_3(PF_6)_3]$, 1463 $[Fe_2(L)_2(L-H)(PF_6)_2]$, 1317 $[Fe_2(L)(L-H)_2(PF_6)]$, 1171 $[Fe_2(L-H)_3]$, 837 $[Fe_2(L-H)_2(F)]$, 818 $[Fe_2(L-H)_2]$, 766 $[Fe(L)(L-H)]$, 409 $[Fe(L-H)]$; positive-ion ESI (MeCN): m/z: 1609 $[Fe_2(L)_3(PF_6)_3]^+$, 1315

$[Fe_2(L)(L-H)_2(PF_6)]^+$, 1256 $[Fe_2(L)_2(PF_6)_3]^+$, 1171 $[Fe_2(L-H)_3]^+$, 732 $[Fe_2(L)_3(PF_6)_2]^{2+}$, 658 $[Fe_2(L)_2(L-H)(PF_6)]^{2+}$, 585 $[Fe_2(L)(L-H)_2]^{2+}$, 439 $[Fe_2(L)_3(PF_6)]^{3+}$, 409 $[Fe(L-H)]^+$, 391 $[Fe_2(L)_2(L-H)]^{3+}$, 355 $[HL]^+$; ^{1}H NMR (CD_3CN, 500 MHz, 298 K): $\delta = 158.3$ (brs, 1H; H^2), 92.1 (s, 1H; N*H*), 42.5 (brs, 1H; H^{im}), 37.9 (s, 1H; H^4), 24.7 (s, 1H; CH_2), 14.6 (s, 2H; H^{Ph}), −5.6 ppm (brs, 2H; H^{Ph}); UV/Vis (MeCN): λ_{max} (ε) = 283 (53200), 313 (58000), 443 (1390), 810 nm (10 $M^{-1}cm^{-1}$); IR data (KBr): $\tilde{\nu}$ = 3622 (w), 3396 (br), 3134 (br), 2934 (w), 2860 (w), 2588 (vw), 1621 (vs), 1600 (sh), 1556 (w), 1501 (m), 1437 (m), 1347 (vw), 1294 (w), 1232 (w), 1208 (w), 1174 (vw), 1144 (vw), 1094 (m), 1011 (w), 848 (vs), 757 (sh), 710 (w), 617 (m), 559 cm^{-1} (s). Orange crystals suitable for X-ray analysis were grown by slow evaporation of a solution of complex **1** in methanol.

$[Fe_2(L)_3][BF_4]_4$ (2): Ligand **L** (0.127 g; 0.36 mmol) and iron(II) chloride tetrahydrate (0.048 g, 0.24 mmol) were stirred in methanol (15 mL) for 40 min. The resulting orange solution was filtered through Celite and treated with methanolic ammonium tetrafluoroborate (excess) to yield an orange product, which was isolated by filtration, washed with methanol and dried in vacuo over P_4O_{10}. The product was then dissoluted in acetonitrile (10 mL). The solution was filtered through Celite, concentrated in vacuo, diluted with methanol (15 mL) and allowed to stay at room temperature for 24 h. An orange polycrystalline powder resulted, which was collected by filtration, washed with cold methanol and finally dried in vacuo under P_4O_{10}. Yield: 65%; elemental analysis calcd (%) for $[Fe_2(C_{21}H_{18}N_6)_3][BF_4]_4 \cdot 2H_2O$: C 48.5, H 3.7, N, 16.2; found: C 48.4, H 3.4, N 16.0; MS (FAB): *m/z*: 1347 $[Fe_2(L)_2(L-H)(BF_4)_2]$, 1259 $[Fe_2(L)(L-H)_2(BF_4)]$, 1171 $[Fe_2(L-H)_3]$, 837 $[Fe_2(L-H)_2(F)]$, 818 $[Fe_2(L-H)_2]$, 766 $[Fe(L)(L-H)]$, 409 [Fe(L-H)]; positive-ion ESI (MeCN): *m/z*: 586 $[Fe_2(L)(L-H)_2]^{2+}$, 420 $[Fe_2(L)_3(BF_4)]^{3+}$, 409 $[Fe(L-H)]^+$, 355 $[HL]^+$; ^{1}H NMR (CD_3CN, 500 MHz, 298 K): $\delta = 159.2$ (brs,1H; H^2), 92.7 (s, 1H; N*H*), 42.9 (brs, 1H; H^{im}), 38.1 (s, 1H; H^4), 24.8 (s, 1H; CH_2), 14.7 (s, 2H; H^{Ph}), −5.7 ppm (brs, 2H; H^{Ph}); UV/Vis (MeCN): λ_{max} (ε) = 285 (54400), 310 (58300), 438 (1400), 822 nm (12 $M^{-1}cm^{-1}$); IR data (KBr): $\tilde{\nu}$ = 3376 (w), 3131 (br), 2932 (w), 2856 (w), 2588 (vw), 1620 (vs), 1599 (s), 1555 (w), 1501 (m), 1437 (m), 1347 (vw), 1294 (m), 1232 (w), 1207 (w), 1082 (vs), 1054 (sh), 935 (vw), 892 (w), 861 (w), 814 (w), 757 (w), 710 (w), 617 (m), 547 (w), 534 (w), 522 (w). X-ray quality, orange crystals of **2** were obtained from a saturated solution of **2** in acetonitrile by diffusion of diisopropyl ether.

$[Fe_2(L)_3][ClO_4]_4$ (3): Ligand **L** (0.096 g; 0.27 mmol) and iron(II) chloride tetrahydrate (0.036 g, 0.18 mmol) were stirred in methanol (15 mL) for 45 min. The resulting orange solution was filtered through Celite and treated with lithium perchlorate (0.4 mmol) dissoluted in MeOH/H_2O (10 mL, 4:1) solvent mixture. An orange product instantaneously formed, and was collected by filtration, washed with methanol and dried in vacuo over P_4O_{10}. Yield: 72%; elemental analysis calcd (%) for $[Fe_2(C_{21}H_{18}N_6)_3][ClO_4]_4 \cdot 2H_2O$: C 47.0, H 3.6, N 15.7; found: C 46.9, H 3.3, N 15.5. MS (FAB): *m/z*: 1473 $[Fe_2(L)_3(ClO_4)_3]$, 1372 $[Fe_2(L)_2(L-H)(ClO_4)_2]$, 1271 $[Fe_2(L)(L-H)_2(ClO_4)]$, 1171 $[Fe_2(L-H)_3]$, 817 $[Fe_2(L-H)(L-2H)]$, 766 $[Fe(L)(L-H)]$, 409 [Fe(L−H)]; positive-ion ESI (MeCN): *m/z* 1470 $[Fe_2(L)_3(ClO_4)_3]^+$, 685 $[Fe_2(L)_3(ClO_4)_2]^{2+}$, 636 $[Fe_2(L)_2(L-H)(ClO_4)]^{2+}$, 586 $[Fe_2(L)(L-H)_2]^{2+}$, 424 $[Fe_2(L)_2(ClO_4)]^{3+}$, 409 $[Fe(L-H)]^+$, 355 $[HL]^+$; ^{1}H NMR (CD_3CN, 500 MHz, 298 K): δ = 158.3 (brs, 1H; H^2), 92.1 (s, 1H; N*H*), 42.5 (brs, 1H; H^{im}), 37.9 (s, 1H; H^4), 24.7 (s, 1H; CH_2), 14.6 (s, 2H; H^{Ph}), −5.6 ppm (brs, 2H; H^{Ph}); UV/Vis (MeCN): λ_{max} (ε) = 286 (57400), 306 (sh), 438 (1410), 834 nm (12 $M^{-1}cm^{-1}$); IR data (KBr): $\tilde{\nu}$ = 3242 (sh), 3135 (br), 2933 (w), 2856 (w), 2588 (vw), 1620 (vs), 1599 (s), 1556 (w), 1501 (s), 1436 (m), 1346 (vw), 1294 (m), 1232 (w), 1207 (w), 1088 (vs), 1008 (m), 969 (vw), 934 (vw), 892 (m), 861 (w), 814 (m), 757 (w), 710 (w), 625 (s), 617 (s), 547 cm^{-1} (w). Orange crystals suitable for X-ray analysis were obtained by slow diffusion, in an H-shaped tube of two 10^{-4} M methanolic solutions containing $[Fe_2(\mathbf{L})_3]Cl_4$ and $LiClO_4$, respectively.

CAUTION! No problems were encountered during the preparation of the perchlorate derivative described above. However, suitable care must be taken when handling such potentially explosive materials.

$[Ni_2(L)_3][PF_6]_4$ (4): Ligand **L** (0.053 g; 0.15 mmol) and nickel(II) chloride hexahydrate (0.024 g, 0.10 mmol) were stirred in methanol (10 mL) for 30 min. The resulting green solution was treated with methanolic ammonium hexafluorophosphate (excess) and filtered through Celite, and the filtrate allowed to standing for 48 h at 4°C. Green crystals formed and were collected by filtration, washed several times with small amounts of cold methanol, and finally dried in vacuo over P_4O_{10}. Yield: 68%; elemental analysis calcd (%) for $[Ni_2(C_{21}H_{18}N_6)_3][PF_6]_4 \cdot 2H_2O$: C 42.1, H 3.2, N 14.0; found: C 41.9, H 3.1, N 13.8; MS (FAB): *m/z*: 1615 $[Ni_2(L)_3(PF_6)_3]$, 1469 $[Ni_2(L)_2(L-H)(PF_6)_2]$, 1323 $[Ni_2(L)(L-H)_2(PF_6)]$, 1177 $[Ni_2(L-H)_3]$, 823 $[Ni_2(L-H)(L-2H)]$, 412 [Ni(L−H)]; positive-ion ESI (MeCN): *m/z*: 1615 $[Ni_2(L)_3(PF_6)_3]^+$, 733 $[Ni_2(L)_3(PF_6)_2]^{2+}$, 660 $[Ni_2(L)_2(L-H)(PF_6)]^{2+}$, 588 $[Ni_2(L)(L-H)_2]^{2+}$, 441 $[Ni_2(L)_3(PF_6)]^{3+}$, 411 $[Ni(L-H)]^+$, 392 $[Ni_2(L)_2(L-H)]^{3+}$, 355 $[HL]^+$; ^{1}H NMR (CD_3CN, 500 MHz, 298 K): δ = 229.0 (brs, 1H; H^2), 93.1 (s, 1H; N*H*), 58.7 (brs, 1H; H^{im}), 40.9 (s, 1H; H^4), 27.5 (s, 1H; CH_2), 15.4 (s, 2H; H^{Ph}), −6.7 ppm (brs, 2H; H^{Ph}). UV/Vis (MeCN): λ_{max} (ε) = 262 (48300), 308 (66200), 554 (24), 900 nm (25 $M^{-1}cm^{-1}$); IR data (KBr): $\tilde{\nu}$ = 3629 (w), 3379 (m), 3139 (w), 3099 (w), 3033 (w), 2933 (w), 2847 (w), 2589 (vw), 1622 (vs), 1600 (s), 1560 (w), 1499 (s), 1438 (m), 1337 (vw), 1289 (m), 1234 (w), 1207 (w), 1174 (vw), 1151 (w), 1094 (m), 1017 (m), 964 (vw), 847 (vs), 755 (sh), 710 (w), 618 (m), 604 (sh), 558 (s), 425 cm^{-1} (vw). Single crystals suitable for X-ray analysis were directly collected from the reaction mixture, after standing at 4°C for 2 days.

$[Co_2(L)_3][PF_6]_4$ (5): Ligand **L** (0.053 g; 0.15 mmol) and cobalt(II) chloride hexahydrate (0.024 g, 0.10 mmol) were stirred in methanol (15 mL) for 30 min. Water (2 mL) was added and the reaction mixture was further stirred for 45 min. The resulting orange solution was treated with potassium hexafluorophosphate (excess) and filtered through Celite, and the filtrate allowed to stay for 24 h at room temperature. Orange crystals formed and were collected by filtration, washed with methanol, and finally dried in vacuo over P_4O_{10}. Yield: 75%; elemental analysis calcd (%) for $[Co_2(C_{21}H_{18}N_6)_3][PF_6]_4 \cdot CH_3OH \cdot H_2O$: C 42.4, H 3.3, N 13.9; found: C 42.4, H 3.0, N 13.8; MS (FAB): *m/z*: 1615 $[Co_2(L)_3(PF_6)_3]$, 1469 $[Co_2(L)_2(L-H)(PF_6)_2]$, 1323 $[Co_2(L)(L-H)_2(PF_6)]$, 1177 $[Co_2(L-H)_3]$, 823 $[Co_2(L-H)(L-2H)]$, 412 [Co(L−H)]; positive-ion ESI (MeCN): *m/z*: 1615 $[Co_2(L)_3(PF_6)_3]^+$, 1174 $[Co_2(L-H)_3]^+$, 734 $[Co_2(L)_3(PF_6)_2]^{2+}$, 662 $[Co_2(L)_2(L-H)(PF_6)]^{2+}$, 588 $[Co_2(L)(L-H)_2]^{2+}$, 442 $[Co_2(L)_3(PF_6)]^{3+}$, 411 $[Co(L-H)]^+$, 392 $[Co_2(L)_2(L-H)]^{3+}$, 355 $[HL]^+$; ^{1}H NMR (CD_3CN, 500 MHz, 298 K): δ = 235.0 (brs, 1H; H^2), 99.6 (s, 1H; N*H*), 52.9 (s, 1H; H^4), 23.8 (brs, 1H; H^{im}), 22.1 (s, 1H; CH_2), 2.0 (s, 2H; H^{Ph}), −19.1 ppm (brs, 2H; H^{Ph}); UV/Vis (MeCN): λ_{max} (ε) = 285 (55600), 318 (38250), 490 nm (42 $M^{-1}cm^{-1}$); IR data (KBr): $\tilde{\nu}$ = 3629 (w), 3379 (m), 3127 (w), 3096 (w), 3031 (w), 2929 (w), 2847 (w), 2589 (vw), 1621v (s), 1600 (s), 1559 (w), 1500 (s), 1439 (m), 1336 (vw), 1290 (m), 1233 (w), 1207 (w), 1174 (vw), 1150 (w), 1094 (m), 1014 (m), 965 (vw), 847 (vs), 756 (sh), 710 (w), 618 (m), 602 (sh), 558 (s), 419 cm^{-1} (vw); X-ray quality, orange crystals were obtained from a saturated 1:1 acetonitrile/acetone solution by slow diffusion of diethyl ether.

$[Mn_2(L)_3][PF_6]_4$ (6): Ligand **L** (0.106 g; 0.3 mmol) and manganese(II) chloride tetrahydrate (0.039 g, 0.2 mmol) were stirred in methanol (15 mL) for 45 min. The resulting yellow solution was treated with methanolic ammonium hexafluorophosphate (excess), filtered through Celite and allowed to stay at room temperature overnight. A pale yellow polycrystalline product formed and was isolated by filtration, washed with methanol, and dried in vacuo over P_4O_{10}. Yield: 74%; elemental analysis calcd (%) for $[Mn_2(C_{21}H_{18}N_6)_3][PF_6]_4 \cdot H_2O$: C 42.7, H 3.2, N 14.2; found: C 42.5, H 3.0, N 14.2; MS (FAB): *m/z*: 1607 $[Mn_2(L)_3(PF_6)_3]$, 1461 $[Mn_2(L)_2(L-H)(PF_6)_2]$, 1315 $[Mn_2(L)(L-H)_2(PF_6)]$, 1169 $[Mn_2(L-H)_3]$, 815 $[Mn_2(L-H)(L-2H)]$, 408 [Mn(L−H)]; positive-ion ESI (MeCN): *m/z*: 731 $[Mn_2(L)_3(PF_6)_2]^{2+}$, 658 $[Mn_2(L)_2(L-H)(PF_6)]^{2+}$, 585 $[Mn_2(L)(L-H)_2]^{2+}$, 408 $[Mn(L-H)]^+$, $[Mn_2(L-H)_2]^{2+}$, 355 $[HL]^+$; UV/Vis (MeCN): λ_{max} (ε) = 267 (51600), 318 nm (112100 $M^{-1}cm^{-1}$); IR data (KBr): $\tilde{\nu}$ = 3631 (w), 3386 (m), 3142 (w), 3102 (w), 3037 (w), 2927 (w), 2848 (w), 2590 (vw), 1623 (vs), 1600 (s), 1556 (w), 1502 (s), 1440 (m), 1347 (vw), 1295 (m), 1232 (w), 1207 (w), 1178 (vw), 1152 (w), 1093 (m), 1005 (m), 970 (vw), 847 (vs), 756 (sh), 710 (w), 620 (m), 602 (sh), 558 (s), 425 cm^{-1} (vw). Yellow crystals suitable for X-ray analysis were grown by slow diffusion of diethyl ether into a solution of complex **6** in 1:1 acetonitrile/acetone.

Crystallography: Crystal data for compounds **1–6** were collected at 180 K with a Siemens-SMART-CCD diffractometer[32] equipped with an Oxford Cryosystem Cryostream Cooler.[33] Refinements were performed with SHELXTL.[34] Systematic absences and/or intensity statistics indicated the appropriate space group. The structures were solved by direct methods with additional light atoms found by Fourier methods. Hydrogen

atoms were added at calculated positions and refined using a riding model with freely rotating methyl groups. Unless otherwise indicated anisotropic displacement parameters were used for all non-hydrogen atoms; hydrogen atoms were given isotropic displacement parameters equal to 1.2 (or 1.5 for methyl hydrogen atoms) times the equivalent isotropic displacement parameter of the atom to which the hydrogen-atom was attached. Details of the data collection and refinement for complexes **1–6** are given in Table 4.

Complex 1: Systematic absences indicated either space group *C*2/*c* or *Cc*. The former was chosen on the basis of intensity statistics and shown to be correct by successful refinement. The asymmetric unit contains one and a half ligands and an iron as the triple helix lies on a two fold axis passing through C214 (special position 4e). There are two PF_6 counterions and three methanol molecules. One methanol molecule is fully occupied (C01–O01), one fully occupied but disordered over two positions (C02A–O02A, C02B–O02B), and one half occupied (C03–O03). Additionally, hydrogen atoms were not found for the disordered methanol molecule and it was refined isotropically. All of the other non-hydrogen atoms were refined anisotropically.

Complex 2: No systematic absences. Space group $P\bar{1}$ was chosen on the basis of intensity statistics and shown to be correct by successful refinement. The asymmetric unit contains the triple helix, four BF_4 counterions, two acetonitrile molecules, two water molecules and one molecule of diisopropyl ether. One BF_4 ion was disordered over two positions (B10A, B10B) in a 50:50 ratio. No hydrogen atoms were found for the two water molecules (O01, O02) and the diisopropyl ether molecule was modelled at 50% occupancy. All non-hydrogen atoms were refined anisotropically, except for the diisopropyl ether molecule and the disordered BF_4 ion which were refined isotropically.

Complex 3: No systematic absences. Space group $P\bar{1}$ was chosen on the basis of intensity statistics and shown to be correct by successful refinement. The asymmetric unit contains the triple helix and four perchlorate counterions, four methanol molecules and a water molecule. The Cl40 perchlorate was disordered over two positions in a 50:50 ratio with Cl4a perchlorate and electron density that was modelled as a water molecule (O07). None of the hydrogen atoms of the various methanol solvent molecules were found. Methanol molecules O01–C01 and O02–C02 were full occupied; O03–C03 and O04–C04 were modelled as half occupied. Methanol molecule O05–C05 was fully occupied, but disordered over two positions O05–C05/O05A–C05A. The occupancies were fixed at 50:50. There was a very disordered water molecule O06, which was modelled over three positions (O06A, O06B and O06C) with the combined occupancy restrained to a value of one (relative occupancies were 0.5, 0.3 and 0.2). The minor component of the disordered Cl40 and methanol O05A–C05A were refined isotropically.

Complex 4: Systematic absences indicated either space group *C*2/*c* or *Cc*. The former was chosen on the basis of intensity statistics and shown to be correct by successful refinement. There are one and a half ligands and a nickel atom in the asymmetric unit as C114 lies on a twofold axis (position 4e). Additionally there are two PF_6 counterions and one whole methanol solvent molecule (C01–O01) and one half occupied (C02–O02). There is also a water molecule modelled as diordered over two positions (O03, O03a). No hydrogen atoms were found for the water molecules.

Complex 5: No systematic absences. The space group $P\bar{1}$ was chosen on the basis of intensity statistics and shown to be correct by successful refinement. The asymmetric unit contains a triple helix, four PF_6 counterions, three acetone molecules and two acetonitrile molecules. The P20 PF_6 is disordered around its equator, in about 7:3 for the two occupancies. One acetonitrile molecule is disordered over two positions (N20-C22, N30-C32) in a ratio of about 8:2.

Complex 6: No systematic absences. Space group $P\bar{1}$ was chosen on the basis of intensity statistics and shown to be correct by successful refinement. The asymmetric unit contains a triple helix, four PF_6 counterions, three molecules of acetone and two of acetonitrile. The P30 PF_6 was disordered around the equator (75:25 major to minor), P40 PF_6 was disordered around phosphorus (50:50) and the acetonitrile molecule (C50A–C52A and C50B–C52B) was disordered over two positions (8:2 major to minor). Additionally, two of the phenyl rings of the diamine units of the ligand were disordered (C215–C220 and C315–C320 by a twisting movement around the C215−C218 axis or C315−C318 axis) over two positions. The occupancies (50:50) of the two sites of disorder were linked as this made chemical sense not to have two parts of the disorder phenyl rings sterically clashing in the helix. These two disordered sets both give rise to similar packing arrangements of the three phenyl rings at that end of the helix. Hydrogen atoms were not located for acetonitrile molecule N40–C42. All non-hydrogen atoms were refined anisotropically, except the minor component of the disordered acetonitile molecule (C50B–C52B).

CCDC-239357–239362 contain the supplementary crystallographic data for this paper. These data can be obtained free of charge via www.ccdc.cam.ac.uk/conts/retrieving.html (or from the Cambridge Crystallographic Data Centre,12 Union Road,Cambridge CB21EZ (UK); fax: (+44) 1223-336-033; or e-mail:deposit@ccdc.cam.ac.uk).

Table 4. Crystallographic data for complexes **1–6** and details of refinement.

	1	**2**	**3**	**4**	**5**	**6**
formula	$C_{68}H_{66}F_{24}Fe_2N_{18}O_5P_4$	$C_{70}H_{67}B_4F_{16}Fe_2N_{20}O_{2.5}$	$C_{67}H_{72}Cl_4Fe_2N_{18}O_{21.5}$	$C_{66}H_{70}F_{24}N_{18}Ni_2O_5P_4$	$C_{76}H_{78}Co_2F_{24}N_{20}O_3P_4$	$C_{76}H_{78}F_{24}Mn_2N_{20}O_3P_4$
M_r	1906.97	1687.38	1726.93	892.70	2017.32	2009.34
T [K]	180(2)	180(2)	180(2)	180(2)	180(2)	180(2)
crystal system	monoclinic	triclinic	triclinic	monoclinic	triclinic	triclinic
space group	*C*2/*c*	$P\bar{1}$	$P\bar{1}$	*C*2/*c*	$P\bar{1}$	$P\bar{1}$
a [Å]	33.490(2)	14.1279(14)	13.5812(11)	33.673(3)	14.6250(6)	14.6954(8)
b [Å]	14.1457(9)	14.5901(14)	18.246(2)	14.1966(12)	18.4440(8)	18.5749(9)
c [Å]	23.0087(14)	21.301(2)	18.261(2)	22.993(2)	18.7820(8)	18.9226(9)
α [°]	90	74.47	78.637(3)	90	77.27	76.924(2)
β [°]	130.8050(10)	75.347(2)	69.401(3)	130.588(6)	67.4920(10)	67.202(2)
γ [°]	90	73.9480(10)	70.2610(10)	90	69.8880(10)	70.349(2)
V [Å^3]	8250.7(9)	3988.8(7)	3971.2(8)	8347.1(12)	4371.9(3)	4456.9(8)
Z	4	2	2	4	2	2
ρ_{calcd} [g^{-1}cm^{-3}]	1.535	1.405	1.144	1.506	1.532	1.497
μ [mm^{-1}]	0.543	0.459	0.582	0.639	0.563	0.463
reflections collected	16596	16279	18304	16334	18002	21024
independent reflections	5371 (R_{int} = 0.1324)	10165 (R_{int} = 0.0747)	12023 (R_{int} = 0.1111)	5428 (R_{int} = 0.0810)	11220 (R_{int} = 0.0653)	13682 (R_{int} = 0.0663)
parameters	557	1016	1049	553	1177	1312
goodness-of-fit on F^2	0.993	0.962	0.944	0.999	1.007	0.948
R_1 [$I > 2\sigma(I)$]	0.0670	0.0779	0.1235	0.0641	0.0785	0.0750
wR_2 [$I > 2\sigma(I)$]	0.1865	0.2171	0.3408	0.1743	0.2146	0.2054

Acknowledgement

This work was supported by an EU Marie Curie Fellowship (F.T.; MCFI-2000-00403). M.J.H. is the Royal Society of Chemistry Sir Edward Frankland Fellow 2004–5. We thank EPSRC and Siemens Analytical Instruments for grants in support of the diffractometer, the EPSRC National Mass Spectrometry Service Centre, Swansea for recording the electrospray mass spectra and Dr. A. J. Clarke for assistance with NMR studies. We thank one of the referees for highlighting the importance of isomorphous structures and Dr. N. W. Alcock for helpful discussions on this subject.

[1] a) J.-M. Lehn, *Supramolecular Chemistry—Concepts and Perspectives*, VCH, Weinheim, **1995**; b) *Comprehensive Supramolecular Chemistry*, (Eds.: J. L. Atwood, J. E. D. Davies, J.-M. Lehn, D. D. MacNicol, F. Vogtle), Pergamon, Oxford, **1996**; c) R. W. Saalfrank, I. Bernt, *Curr. Opin. Solid State Mater. Sci.* **1998**, *3*, 407–413; d) D. Philp, J. F. Stoddart, *Angew. Chem.* **1996**, *108*, 1242–1286; *Angew. Chem. Int. Ed. Engl.* **1996**, *35*, 1155–1196; e) M. Albrecht, *J. Inclusion Phenom. Macrocyclic Chem.* **2000**, *36*, 127–151; f) C. Dietrich-Buchecker, G. Rapenne, J. P. Sauvage, *Coord. Chem. Rev.* **1999**, *186*, 167–176; g) M. Fujita, *Acc. Chem. Res.* **1999**, *32*, 53–61; h) B. Olenyuk, A. Fechtenkotter, P. J. Stang, *J. Chem. Soc. Dalton Trans.* **1998**, 1707–1728; i) D. L. Caulder, K. N. Raymond, *Acc. Chem. Res.* **1999**, *32*, 975–982; j) D. W. Johnson, K. N. Raymond, *Supramol. Chem.* **2001**, *13*, 639–659; k) E. C. Constable, *Prog. Inorg. Chem.* **1994**, *42*, 67–138; l) R. W. Saalfrank, I. Bernt, *Curr. Opin. Solid State Mater. Sci.* **1998**, *3*, 407–413.

[2] a) C. Dietrich-Buchecker, M. C. Jimenez-Molero, V. Sartor, J.-P. Sauvage, *Pure Appl. Chem.* **2003**, *75*, 1383–1393; b) J. P. Collin, C. Dietrich-Buchecker, P. Gavina, M. C. Jimenez-Molero, J.-P. Sauvage, *Acc. Chem. Res.* **2001**, *34*, 477–487; c) J. C. Chambron, J.-P. Sauvage, *Chem. Eur. J.* **1998**, *4*, 1362–1366; d) P. N. W. Baxter, H. Sleiman, J.-M. Lehn, K. Rissanen, *Angew. Chem.* **1997**, *109*, 1350–1352; *Angew. Chem. Int. Ed. Engl.* **1997**, *36*, 1294–1296; e) L. Raehm, J. P. Sauvage, *Struct. Bond.* **2001**, *99*, 55–78.

[3] a) C. Dietrich-Buchecker, G. Rapenne, J. P. Sauvage, *Coord. Chem. Rev.* **1999**, *186*, 167–176; b) C. Dietrich-Buchecker, G. Rapenne, J. P. Sauvage, A. De Cian, J. Fischer, *Chem. Eur. J.* **1999**, *5*, 1432–1439; c) S. C. J. Meskers, H. P. J. M. Dekkers, G. Rapenne, J. P. Sauvage, *Chem. Eur. J.* **2000**, *6*, 2129–2134 .

[4] a) L. J. Childs, M. J. Hannon, *Supramol. Chem.* **2004**, *16*, 7–22; b) C. Piguet, G. Bernardinelli, G. Hopfgartner, *Chem. Rev.* **1997**, *97*, 2005–2062; c) M. Albrecht, *Chem. Rev.* **2001**, *101*, 3457–3497; d) A. F. Williams, *Pure Appl. Chem.* **1996**, *68*, 1285–1289.

[5] a) M.-T. Youinou, N. Rahmouni, J. Fischer, J. A. Osborn, *Angew. Chem.* **1992**, *104*, 771–773; *Angew. Chem. Int. Ed. Engl.* **1992**, *31*, 733–735; b) P. N. W. Baxter, J.-M. Lehn, J. Fischer, M.-T. Youinou, *Angew. Chem.* **1994**, *106*, 2432–2435; *Angew. Chem. Int. Ed. Engl.* **1994**, *33*, 2284–2287; c) M. Ruben, E. Breuning, M. Barboiu, J. P. Gisselbrecht, J. M. Lehn, *Chem. Eur. J.* **2003**, *9*, 291–299; d) D. M. Bassani, J. M. Lehn, S. Serroni, F. Puntoriero, S. Campagna, *Chem. Eur. J.* **2003**, *9*, 5936–5946; e) L. H. Uppadine, J.-M. Lehn, *Angew. Chem.* **2004**, *116*, 242–245; *Angew. Chem. Int. Ed.* **2004**, *43*, 240–243; f) L. K. Thompson, C. J. Matthews, L. Zhao, Z. Xu, D. O. Miller, C. Wilson, M. A. Leeh, J. A. K. Howard, S. L. Heath, A. G. Whittaker, R. E. P. Winpenny, *J. Solid State Chem.* **2001**, *159*, 308–320.

[6] a) H. Sleiman, P. N. W. Baxter, J.-M. Lehn, K. Airola, K. Rissanen, *Inorg. Chem.* **1997**, *36*, 4734–4742; b) H. Sleiman, P. Baxter, J.-M. Lehn, K. Rissanen, *J. Chem. Soc. Chem. Commun.* **1995**, 715–716.

[7] a) M. Fujita, K. Ogura, *Coord. Chem. Rev.* **1996**, *148*, 249–264; b) M. Fujita, T. Kusukawa, *Angew. Chem.* **1998**, *110*, 3327–3329; *Angew. Chem. Int. Ed.* **1998**, *37*, 3142–3144; c) T. Kusukawa, M. Yoshizawa, M. Fujita, *Angew. Chem.* **2001**, *113*, 1931–1936; *Angew. Chem. Int. Ed.* **2001**, *40*, 1879–1884; d) B. Linton, A. D. Hamilton, *Chem. Rev.* **1997**, *97*, 1669–1680; e) J. K. M. Sanders, *Pure Appl. Chem.* **2000**, *72*, 2265–2274; f) P. D. Beer, E. J. Hayes, *Coord. Chem. Rev.* **2003**, *240*, 167–189; g) M. Albrecht, O. Blau, *Chem. Commun.* **1997**, 345–346; h) B. Hasenknopf, J.-M. Lehn, N. Boumediene, A. DupontGervais, A. VanDorsselaer, B. O. Kneisel, D. Fenske, *J. Am. Chem. Soc.* **1997**, *119*, 10956–10962; i) B. Hasenknopf, J.-M. Lehn, B. O. Kneisel, G. Baum, D. Fenske, *Angew. Chem.* **1996**, *108*, 1987–1989; *Angew. Chem. Int. Ed. Engl.* **1996**, *35*, 1838–1840; j) P. L. Jones, K. J. Byrom, J. C. Jeffery, J. A. McCleverty, M. D. Ward, *Chem. Commun.* **1997**, 1361–1362; k) J. S. Fleming, K. L. V. Mann, C. A. Carraz, E. Psillakis, J. C. Jeffery, J. A. McCleverty, M. D. Ward, *Angew. Chem.* **1998**, *110*, 1315–1318; *Angew. Chem. Int. Ed.* **1998**, *37*, 1279–1281; l) A. Bilyk, M. M. Harding, *J. Chem. Soc. Dalton Trans.* **1994**, 77–82; m) A. Bilyk, M. M. Harding, P. Turner, T. W. Hambley, *J. Chem. Soc. Dalton Trans.* **1995**, 2549–2553; n) A. Bilyk, M. M. Harding, *J. Chem. Soc. Chem. Commun.* **1995**, 1697–1698; o) M. A. Houghton, A. Bilyk, M. M. Harding, P. Turner, T. W. Hambley, *J. Chem. Soc. Dalton Trans.* **1997**, 2725–2733.

[8] a) M. J. Hannon, V. Moreno, M. J. Prieto, E. Moldrheim, E. Sletten, I. Meistermann, C. J. Isaac, K. J. Sanders, A. Rodger, *Angew. Chem.* **2001**, *113*, 903–908; *Angew. Chem. Int. Ed.* **2001**, *40*, 880–884; b) I. Meistermann, V. Moreno, M. J. Prieto, E. Moldrheim, E. Sletten, S. Khalid, M. Rodger, J. Peberdy, C. J. Isaac, A. Rodger, M. J. Hannon, *Proc. Natl. Acad. Sci. USA* **2002**, *99*, 5069–5074; c) E. Moldrheim, M. J. Hannon, I. Meistermann, A. Rodger, E. Sletten, *J. Biol. Inorg. Chem.* **2002**, *7*, 770–780; d) M. J. Hannon, A. Rodger, *Pharmaceutical Visions* **2002**, autumn issue, p. 14.

[9] a) A. El-ghayoury, L. Douce, A. Skoulios, R. Ziessel, *Angew. Chem.* **1998**, *110*, 2327–2331; *Angew. Chem. Int. Ed.* **1998**, *37*, 2205–2208; b) L. Douce, R. Ziessel, *Mol. Cryst. Liq. Cryst.* **2001**, *362*, 133–145; c) R. Ziessel, *Coord. Chem. Rev.* **2001**, *216*, 195–223.

[10] O. Kahn, *Molecular Magnetism*, VCH, Wenheim, **1993**.

[11] a) H. Toftlund, *Monatsh. Chem.* **2001**, *132*, 1269–1277; b) H. Toftlund, *Coord. Chem. Rev.* **1989**, *94*, 67–108; c) P. Gütlich, Y. Garcia, H. A. Goodwin, *Chem. Soc. Rev.* **2000**, *29*, 419–427; d) B. A. Leita, B. Moubaraki, K. S. Murray, J. P. Smith, J. D. Cashion, *Chem. Commun.* **2004**, 156–157.

[12] a) O. Kahn, C. J. Martinez, *Science* **1998**, *279*, 44–48; b) Y. Bretonnière, M. Mazzanti, J. Pécaut, M. M. Olmstead, *J. Am. Chem. Soc.* **2002**, *124*, 9012–9013; c) C. Cadiou, M. Murrie, C. Paulsen, V. Villar, W. Wernsdorfer, R. E. P. Winpenny, *Chem. Commun.* **2001**, 2666; d) O. Kahn, J. Kröber, C. Jay, *Adv. Mater.* **1992**, *4*, 718; e) V. Niel, J. M. Martinez-Agudo, M. Carmen Muñoz, A. B. Gaspar, J. A. Real, *Inorg. Chem.* **2001**, *40*, 3838–3839.

[13] a) J.-F. Létard, P. Guionneau, E. Codjovi, O. Lavastre, G. Bravic, D. Chasseau, O. Kahn, *J. Am. Chem. Soc.* **1997**, *119*, 10861–10862; b) J.-F. Létard, S. Montant, P. Guionneau, P. Martin, A. Le Calvez, E. Freysz, D. Chasseau, R. Lapouyade, O. Kahn, *Chem. Commun.* **1997**, 745–746.

[14] a) M. Yamada, M. Ooidemizu, Y. Ikuta, S. Osa, N. Matsumoto, S. Iijuma, M. Kojima, F. Dahan, J. P. Tuchagues, *Inorg. Chem.* **2003**, *42*, 8406–8416; b) Y. Sunatsuki, Y. Ikuta, N. Matsumoto, H. Ohta, M. Kojima, S. Iijuma, S. Hayami, Y. Maeda, S. Kaizaki, F. Dahan, J. P. Tuchagues, *Angew. Chem.* **2003**, *115*, 1652–1656; *Angew. Chem. Int. Ed.* **2003**, *42*, 1614–1618.

[15] a) J. A. Real, A. B. Gaspar, V. Niel, M. C. Muñoz, *Coord. Chem. Rev.* **2003**, *236*, 121–141; b) G. J. Halder, C. J. Kepert, B. Moubaraki, K. S. Murray, J. D. Cashion, *Science* **2002**, *298*, 1762–1765; c) V. Ksenofontov, A. B. Gaspar, V. Niel, S. Reiman, J. A. Real, P. Gütlich, *Chem. Eur. J.* **2004**, *10*, 1291–1298.

[16] a) S. G. Telfer, B. Bocquet, A. F. Williams, *Inorg. Chem.* **2001**, *40*, 4818–4820; b) L. J. Charbonniere, A. F. Williams, C. Piguet, G. Bernardelli, E. Rivara-Minten, *Chem. Eur. J.* **1998**, *4*, 485–493.

[17] a) M. Ruben, E. Breunin, J.-M. Lehn, V. Ksenofontov, F. Renz, P. Gütlich, G. B. M. Vaughan, *Chem. Eur. J.* **2003**, *9*, 4422–4429; b) E. Breuning, M. Ruben, J.-M. Lehn, F. Renz, Y. Garcia, V. Ksenofontov, P. Gütlich, E. Wegelius, K. Rissanen, *Angew. Chem.* **2000**, *112*, 2563–2565; *Angew. Chem. Int. Ed.* **2000**, *39*, 2504–2507.

[18] a) M. J. Hannon, C. L. Painting, J. Hamblin, A. Jackson, W. Errington, *Chem. Commun.* **1997**, 1807–1808; b) M. J. Hannon, I. Meistermann, C. J. Isaac, C. Blomme, J. Aldrich-Wright, A. Rodger, *Chem. Commun.* **2001**, 1078–1079.

[19] a) M. J. Hannon, S. Bunce, A. J. Clarke, N. W. Alcock, *Angew. Chem.* **1999**, *111*, 1353–1355; *Angew. Chem. Int. Ed.* **1999**, *38*, 1277–1278; b) L. J. Childs, N. W. Alcock, M. J. Hannon, *Angew. Chem.* **2001**, *113*, 1113–1115; *Angew. Chem. Int. Ed.* **2001**, *40*, 1079–1081;

c) J. Hamblin, L. J. Childs, N. W. Alcock, M. J. Hannon, *J. Chem. Soc. Dalton Trans.* **2002**, 164–169; d) L. J. Childs, N. W. Alcock, M. J. Hannon, *Angew. Chem.* **2002**, *114*, 4418–4421; *Angew. Chem. Int. Ed.* **2002**, *41*, 4244–4247; e) J. Hamblin, A. Jackson, N. W. Alcock, M. J. Hannon, *J. Chem. Soc. Dalton Trans.* **2002**, 1635–1641; f) F. Tuna, G. Clarkson, N. W. Alcock, M. J. Hannon, *Dalton Trans.* **2003**, 2149–2155; g) F. Tuna, J. Hamblin, G. Clarkson, W. Errington, N. W. Alcock, M. J. Hannon, *Chem. Eur. J.* **2002**, *8*, 4957–4964; h) M. J. Hannon, C. L. Painting, N. W. Alcock, *Chem. Commun.* **1999**, 2023–2024; i) A. Lavalette, J. Hamblin, A. Marsh, D. M. Haddleton, M. J. Hannon, *Chem. Commun.* **2002**, 3040–3041; j) F. Tuna, J. Hamblin, A. Jackson, G. Clarkson, N. W. Alcock, M. J. Hannon, *Dalton Trans.* **2003**, 2141- 2148; k) M. Pascu, F. Tuna, E. Kolodziejczyk, G. I. Pascu, G. Clarkson, M. J. Hannon, *Dalton Trans.* **2004**, 1546- 1555.

[20] A. Lavalette, F. Tuna, G. Clarkson, N. W. Alcock, M. J. Hannon, *Chem. Commun.* **2003**, 2666–2667.

[21] a) U. Ziener, E. Breuning, J-M. Lehn, E. Wegelius, K. Rissanen, G. Baum, D. Fenske, G. Vaughan, *Chem. Eur. J.* **2000**, *6*, 4132–4139; b) E. Breuning, U. Ziener, J.-M. Lehn, E. Wegelius, K. Rissanen, *Eur. J. Inorg. Chem.* **2001**, 1515–1521.

[22] Z. Qin, M. C. Jennings, R. J. Puddephatt, *Chem. Commun.*, **2001**, 2676–2677.

[23] While distance alone does not give an accurate picture of hydrogen-bonding interactions, it is used here to qualitatively assess the extent of N–H···X interactions. Interaction distances up to 3.0 Å are listed, but are not intended to imply strong hydrogen bonds at such distances.

[24] One of the tetrafluoroborate anions is disordered over two positions, but makes the short bridging contacts in both of these positions. In the second orientation this tetrafluoroborate uses one fluorine atom to make one hydrogen bond to one helix and this fluorine atom and an additional one to make a pair of hydrogen bonds to an NH of the adjacent helix. The F···HN distances to the additional position are 2.13 Å for the single hydrogen bond and 2.08 and 2.60 Å for the pair. For clarity this additional position is not shown in the diagram.

[25] E. C. Constable, G. Baum, E. Bill, R. Dyson, R. van Eldick, D. Fenske, S. Kaderli, D. Morris, A. Neubrand, M. Neuburger, D. R. Smith, K. Wieghardt, M. Zehnder, A. D. Zuberbühler, *Chem. Eur. J.* **1999**, *5*, 498–508.

[26] E. C. Constable, C. E. Housecroft, T. Kulke, C. Lazzarini, E. R. Schofield, Y. Zimmermann, *J. Chem. Soc. Dalton Trans.* **2001**, 2864–2871.

[27] E. C. Constable, M. J. Hannon, D. A. Tocher, *J. Chem. Soc. Dalton Trans.* **1993**, 1883–1890.

[28] J. Jeftic, R. Hinek, S. C. Capelli, A. Hauser, *Inorg. Chem.* **1997**, *36*, 3080–3087.

[29] B. N. Figgis, J. Lewis, F. E. Mabbs, G. A. Webb, *J. Chem. Soc. A* **1966**, 1411–1421.

[30] J. C. Noveron, M. S. Lah, R. E. Del Sesto, A. M. Arif, J. S. Miller, P. J. Stang, *J. Am. Chem. Soc.* **2002**, *124*, 6613–6625.

[31] a) J. Hossain, M. Yamasaki, M. Mikuriya, A. Kuribayashi, H. Sakiyama, *Inorg. Chem.* **2002**, *41*, 4058–4062; b) F. Tuna, S. Golhen, L. Ouahab, J.-P. Sutter, *C. R. Chimi.* **2003**, *6*, 377–383.

[32] SMART user's manual, Siemens Industrial Automation, Madison, WI, **1994**.

[33] J. Cosier, A. M. Glazer, *J. Appl. Crystallogr.* **1986**, *19*, 105–107.

[34] G. M. Sheldrick, *Acta Crystallogr. A* **1990**, *46*, 467–473.

Received: May 25, 2004
Published online: October 7, 2004

